Rochester Institute of Technology

RIT Digital Institutional Repository

7-18-2017

Enhanced Pool Boiling Heat Transfer by Flow Modulation and Contact Line Augmentation over Cylindrical Tubes

Indranil M. Joshi
imj5686@rit.edu

Follow this and additional works at: https://repository.rit.edu/theses

R.I.T

Enhanced Pool Boiling Heat Transfer by Flow Modulation and Contact Line Augmentation over Cylindrical Tubes

By: Indranil M. Joshi

A Thesis Submitted in Partial Fulfillment of the Requirement for the Degree of Master of Science in Mechanical Engineering

Thermal Analysis, Microfluidics and Fuel Cell Lab

Department of Mechanical Engineering

Kate Gleason College of Engineering

ROCHESTER INSTITUTE OF TECHNOLOGY

Rochester, NY

July 18th, 2017

Enhanced Pool Boiling Heat Transfer by Flow Modulation and Contact Line Augmentation over Cylindrical Tubes

By: Indranil M. Joshi

A Thesis Submitted in Partial Fulfillment of the Requirements for the Degree of Master of Science in Mechanical Engineering

Department of Mechanical Engineering

Kate Gleason College of Engineering

Rochester Institute of Technology

Approved By:

Dr. Satish G. Kandlikar

Thesis Advisor   *Date*

Department of Mechanical Engineering

Dr. Agamemnon Crassidis

Department Representative, Thesis Committee Member   *Date*

Department of Mechanical Engineering

Dr. Michael Schrlau

Thesis Committee Member   *Date*

Department of Mechanical Engineering

Dr. Kathleen Lamkin-Kennard

Thesis Committee Member   *Date*

Department of Mechanical Engineering

Abstract

The miniaturization trend in electronics has spurred the development of efficient thermal management solutions. Single phase techniques are reliable but are limited by large fluid temperature differences and pressure drop. Two phase cooling has very little pressure drop with large heat absorption capacity. Boiling stands out as one of the most effective methods of heat dissipation which utilizes phase change. However, the design of two-phase systems is limited by the critical heat flux condition where a vapor layer prevents the liquid from contacting the heater surface. The current research study is directed towards increasing the CHF and maintaining low wall superheats to design efficient heat removal systems.

In this study, different surface modification techniques are studied with an aim to identify various mechanisms that affect the heat transfer. Different surface enhancements in the form of Circumferential rectangular microchannels(CRM) and fin are used over cylindrical surface. Cylindrical tube with outer diameter of 15 mm was used for testing with water as working fluid. Tubular surface with fin attached performed the best yielding the CHF of 115 W/cm^2 at wall superheat of 18°C which translated to an enhancement of 76%. The best performance of 110 W/cm^2 at 9 ^{o}C without reaching CHF was obtained amongst CRM.

Different mechanisms were identified by analyzing the results from pool boiling experiments. Area enhancement and contact line substantially affected the heat transfer performance in CRM. Area enhancement increased performance by providing additional area for heat transfer. Contact line region has higher heat flux. Single bubble growing over multiple grooves has increased contact line density which increases heat transfer

performance. Increment in CHF was obtained by employing any one of these surface enhancements.

High speed imaging enabled to analyze the behavior of bubble after nucleation on the fin surface thus deciphering the flow modulation over the cylindrical surface. Presence of bubble diverter at the bottom surface ensured higher evaporative momentum force towards the cylindrical surface. This displaced nucleating bubble at the bottom away from the fin, enabling liquid to rewet the surface. This allowed the formation of separate liquid vapor pathways which resulted in increased performance.

ACKNOWLEDGEMENT

I would like to take this opportunity to thank everyone for their support and guidance. I am extremely grateful to Dr. Satish G. Kandlikar for giving me the opportunity to be a part of Thermal Analysis, Micro fluidics and Fuel Cell Lab and work under his guidance. You have been a constant source of encouragement. I feel privileged to have worked under your guidance and learned from you which only made me a better engineer. I would also like to thank the committee members for taking out the time to review and evaluate my thesis. I am grateful to Craig Arnold and Jan Maneti from RIT's Machine shop for helping me with all the tedious machining, all TAMFL members for their support.

I am indebted to Dr. P.R. Mukund for his teachings and guidance which have helped me become a better person. I am grateful to Kevin Hill and his family, Donna and Tom Anderson, for their hospitality and care.

I would like to thank all my friends for being there for me through thick and thin. And lastly, I would like to thank my wonderful family for being so encouraging, supportive, thoughtful and kind and for believing in me when I couldn't. I am where I am because of you. Thank you for everything!

Table of Contents

List of Figures

List of Tables

Nomenclature

V	Voltage, V
I	Current, A
q_h	Heat input, W
$q_{a,l}$	Axial heat loss, W
q_r	Heat input in radial direction, W
A_s	Surface area at outer diameter, m^2
r_2	Outer radius of test section, m
r_1	Radius at which all the thermocouples are placed, m
L	Length of test section, m
$T_1 - T_4$	Temperature of all thermocouples at r_1, ^oC
T_5	Temperature of water, ^oC
T_{avg}	Average temperature of thermocouples at radius r_1, ^oC
T_s	Surface temperature, ^oC
h	Heat transfer coefficient, $kW/m^{2o}C$
q_r''	Radial heat flux, W/cm^2
U_{Ts}	Uncertainty in surface temperature, ^oC
U_{Tavg}	Uncertainty in average temperature, ^oC
U_{qr}	Uncertainty in heat input in radial direction, W
U_{qr}''	Uncertainty in radial heat flux, W/cm^2
U_h	Uncertainty in heat transfer coefficient, kW/m^2

Abbreviations

CHF   Critical Heat flux

CRM   Circumferential rectangular microchannels

ARM   Axial rectangular microchannels

EMF   Evaporative momentum force

1.0 Introduction

Tubular surfaces are extensively used in heat exchangers and air conditioning industries. Cylindrical surfaces are very effective for transferring heat from one medium to another. While it is an efficient configuration for heat transfer, it is limited by the input conditions of the cooling medium and sensible heat transfer. However, using fluid at saturated condition with phase change has a significant impact on increasing the heat transfer performance of system. This is because convective heat transfer coefficients of boiling for all fluids are significantly higher compared to all convective heat transfer modes.

Heat transfer can be classified into three different mechanisms, namely, conduction, convection and radiation. Conduction can be observed within solid bodies and fluids which are stagnant/ stationary. When a part of material encounters hot material, the atoms in that region gain energy and they start vibrating. Thus, passing on the energy to the adjacent atoms. In convection, there is free flow of fluid with gain of energy. In convection, the layer of fluid which is in contact with the heater surface moves up allowing other layers with high density to settle down and absorb heat. Heat transfer by convection can be forced or natural. Radiation takes places in vacuum and does not require any medium for heat transfer. Heat is transferred in the form of short waves.

1.1 Boiling

Boiling is effective way of cooling systems. It is technique which relies on phase change of fluid for dissipating heat from the system. The phase change for any fluid has a tremendous heat absorption capacity. High heat transfer coefficients with little variance in operating temperatures makes it a very attractive option for cooling. The upper limit

however for such heat transfer is limited by Critical Heat Flux (CHF) when the surface temperature spikes up suddenly to a couple hundred degrees. Heat transfer by boiling is characterized by basic boiling curve which follows multiple regimes as shown in figure 1.
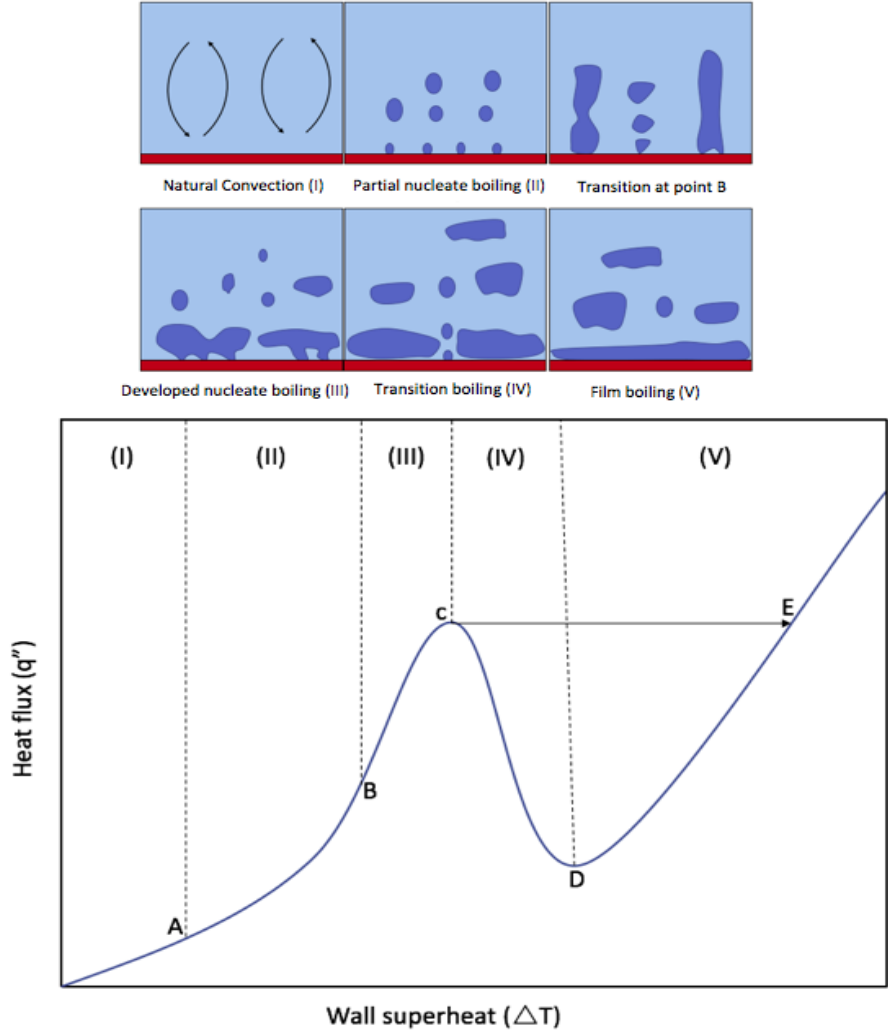
Figure 1 Pool boiling curve with different boiling regimes

Natural Convection

The first mode of heat transfer is natural convection. Here the wall superheat is insufficient to allow nucleation of bubbles on the heater surface. With further increase in heat flux the wall superheat becomes significant to allow formation of small vapor bubbles over the heater surface. This is known as Onset of Nucleate Boiling.

Nucleate boiling

With the onset of nucleate boiling, discrete bubbles from various locations are seen nucleating on heater surface. The frequency of these bubbles and active nucleation sites increase with rise in surface temperature and heat flux. This region is called partial nucleate boiling and is marked with a steep slope in region (II) of figure 1. After increase in heat flux to a certain point the nucleated bubbles start to coalesce and vertical vapor jets are seen coming out from the heater surface. This point is known as the transition point which is shown as point B in figure 1. The region between B and C is known as developed nucleate region. In this phase nucleated bubbles coalesce vertically as well as horizontally with other bubbles. This phase is marked with mushroom like vapor structures. With further increase in heat flux Point C is reached which is marked by sudden rise in temperature leading to Critical Heat Flux (CHF). Critical Heat Flux (CHF) in pool boiling curve is seen as a sudden jump from point C to point E.

Film boiling

At Critical Heat Flux (CHF), the heater surface is completely encapsulated by a vapor film and heat is transferred through the vapor layer that is formed. The vapor layer acts as an insulation resulting in minimum heat transfer, hence sudden increase in temperature is

seen. With further decrease in heat flux the wall superheat also decreases. This goes on until the vapor layer collapses due to insufficient heat flux.

Transition boiling

After the collapse of vapor film the heat rapidly transfers from region (IV) to (II) through (III). This sudden passage from phase IV is known as Transition boiling. Transition boiling is very unstable as the wall superheat increases with decrease in heat flux. Hence it is very difficult to achieve a steady state in transition boiling unless the wall superheat of the heater surface can be controlled.

CHF is the upper limit for any two-phase cooling system. To increase the capacity of Two phase cooling systems it is very important to increase the point of CHF for the system while decreasing the wall superheat. This also increases the Heat transfer coefficient of the system, thus making it more efficient. The presented work deals with using various methods for enhancing the CHF of the system while decreasing the wall superheat thus making it more efficient.

2.0 Literature Review

Two phase cooling has garnered attention of researchers with its ability to dissipate large amount of heat over small area. The formation of bubbles when liquid in saturated condition contacts the heated surface is the main source of heat transfer. Over the years many pool boiling experiments have been performed to understand this bubble formation and pool boiling curve with the aim to increase the critical heat flux (CHF) condition as high as possible.

To increase the Critical heat flux point (CHF), various methods have been used over the years. Annular enhancement[1–7], Nano fluids[8–14], reentrant cavities[15–17], orientation[18–20] and open microchannels/extended surfaces[21–25] are used to increase heat transfer performance.
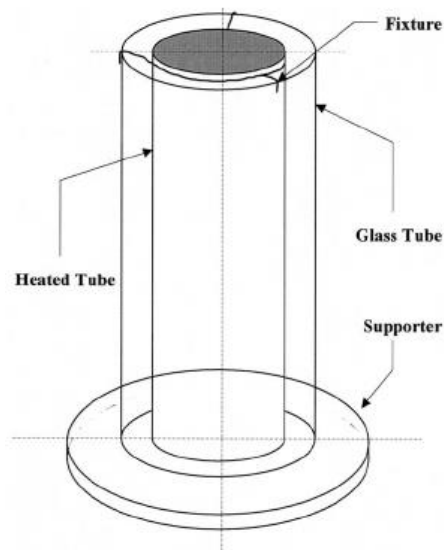
Figure 2 Schematic of annular flow test section[1]

Annular enhancement was studied extensively by various researchers[1–7]. In annular enhancement, heated tube is covered on the outside by another tube as shown in figure

2. It was observed that the heat transfer in such enhancement is governed by the gap size between both the tubes and greater heat transfer is observed with decrease in gap size. Higher heat transfer coefficients were observed at moderate heat fluxes and this was more profound in tubes with closed bottoms. Kang[3] studied the effect of putting a step on the outside tube as shown in figure 3. It was observed that the heat transfer performance deteriorated when the outside tube with a step was used compared to a single unrestricted tube on the outside. This was mainly due to decreased liquid agitation and generation of big bubbles at the stepped region.
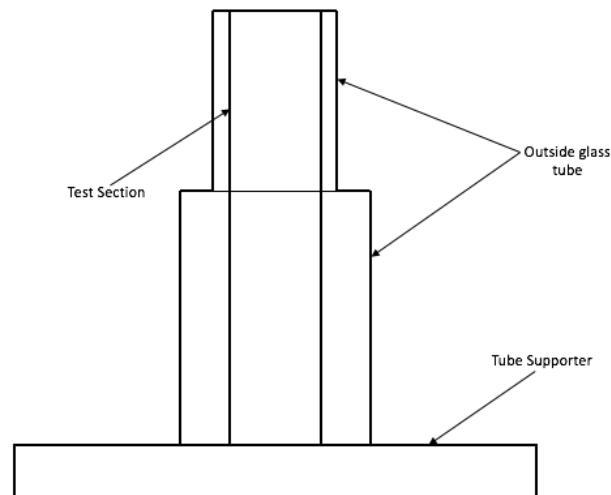
Figure 3 Schematic of annular flow test section with a step in outside glass tube

Impact of Nano fluids on heat transfer performance of the system was studied by few researchers[8–14]. Narayan et al.[8,9] studied the effect of Nano particles over different orientations of tube. They concluded that the horizontal arrangement gave the highest performance while inclined orientation yielded lowest performance, also Nano particles with larger particle size resulted in highest performance amongst all. They also studied effect of surface roughness of heater along with the effect of concentration of Nano fluids

on heat transfer performance of the system. It was seen that the heater with highest surface roughness yields maximum result even at low concentration.

Reentrant cavities are the surfaces created with appropriate gaps which act as nucleation sites facilitating early nucleation. Various researchers[15–17] studied reentrant cavities extensively. In 2002 Kulenovic et al.[15] studied the effect of reentrant cavities with hydrocarbon propane as the working fluid. They developed various boiling parameters, bubble departure diameter along with bubble generation frequency and bubble flow velocity for low heat fluxes using high speed imaging and digital image processing. Ji et al.[16] investigated heat transfer performance on four different surfaces. One surface was plain while remaining three surfaces were enhanced with Integral fin, pyramid and reentrant cavities as shown in figure 4.
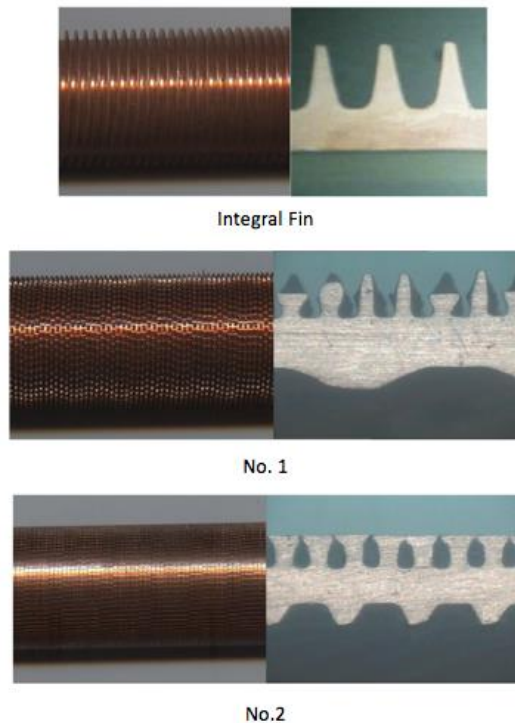
Figure 4 Geometries of enhanced tubes by Ji et al.[16]

No 1 tube had fins of pyramid profiles and were helically arranged located side by side while No.2 had flattened base integral fins with connecting tunnels under the surface. It was seen that the No.2 chip yielded superior performance over all of them. Memory et al.[17] tested pool boiling performance for various enhanced tubes which contained five finned and three reentrant cavities tubes in pure R-114 and R-114-oil mixtures. Figure 5 shows some of the enhanced tubes used for testing.
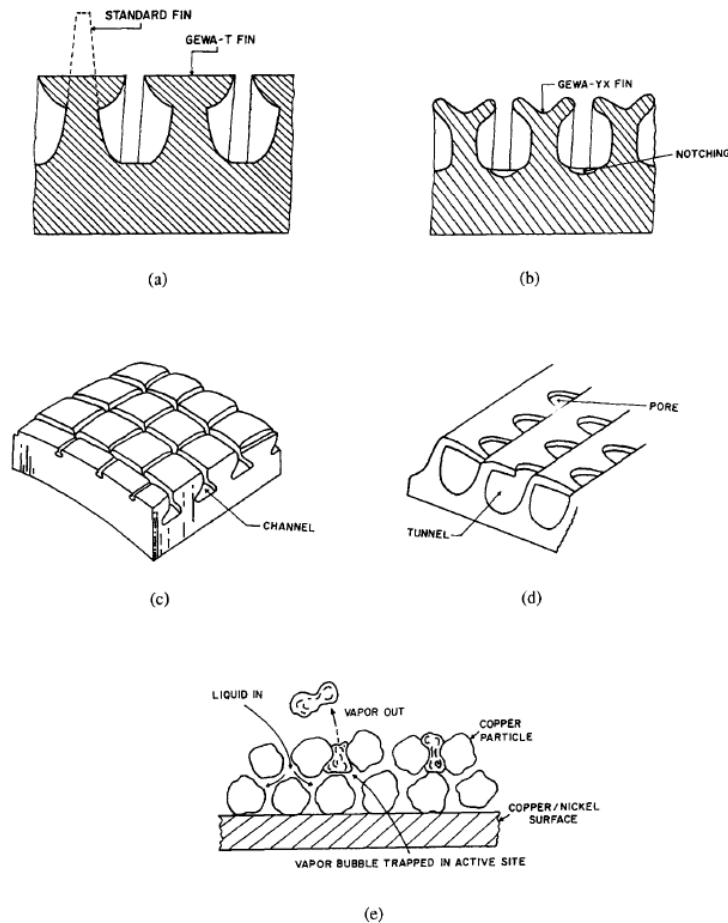
Figure 5 Enhanced tubes tested. (a) Finned (GEWA-K and GEWA-T). (b) Finned (GEWA-YX). (c)Structured (TURBO-B). (d) Structured (THERMOEXCEL-HE). (e) Porous (HIGH FLUX) by Memory et al.[17]

Tubes a, b and c were finned tubes which were commercially available while tubes d and e were structured and porous tubes respectively. It was seen that for pure R-114, finned

tubes typically provided enhancement between 3 to 4 and reentrant cavities initially provided enhancement of 10 for low heat fluxes which later decreased to 4 at higher heat fluxes. Addition of oil in R-114 however caused steady decrease in performance for reentrant cavities but it increased initially and then dropped off for finned surface.

Heater orientation has a considerable effect on the heat transfer performance of the system. Kang[18] studied the effect of tube inclination on pool boiling heat transfer. He studied the effects of seven different angles with two tubes of different diameters. It is seen that the pool boiling performance is drastically affected with change in angle of the heater. Maximum heat transfer coefficients were observed when the heater was near horizontal position and minimum heat transfer coefficients were observed for angles close to vertical orientation as shown in figure 6.
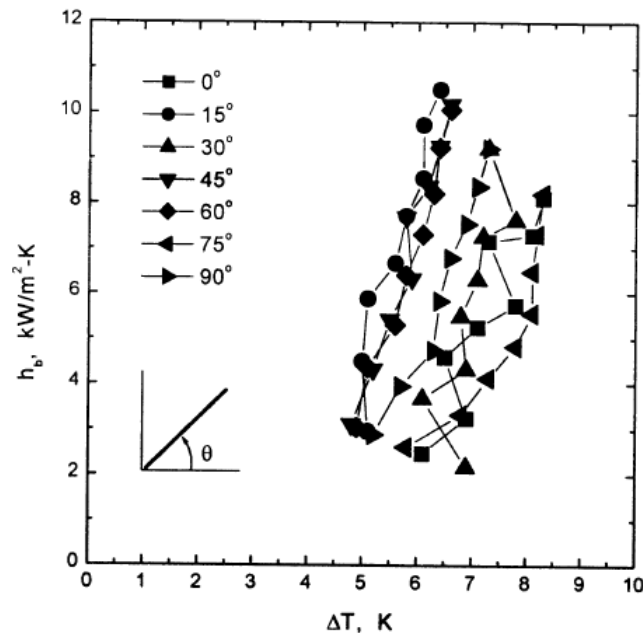
Figure 6 Heat transfer coefficient vs. wall superheat (D=12.7 mm) by Kang[18]

The possible cause for increased heat transfer performance is decrease in bubble slug formation with easy access of liquid to the surface. Sateesh et al.[19] also studied the effect of surface inclination on pool boiling heat transfer with different fluids, tube diameters and roughness values for heater. They found that as the orientation of heater goes from vertical to horizontal, the temperature at top and bottom increases and decreases respectively which results in high heat transfer coefficients at bottom and low heat transfer coefficients on top surface. They noticed that this increase and decrease of heat transfer is such that they compensate for each other and the total heat transfer variation is minimum.

2.1 Effect of Open Microchannels

In 2011, Cooke and Kandlikar [21,22] tested copper and silicon open microchannels in pool boiling configuration for a wide range of channel widths and depths. From the high-speed images captured, they reported that the nucleation of the bubble starts at the bottom surface between two fins and with time the bubble starts moving towards the microstructure wall. The bubble traces the sidewall regions and eventually departs from adjacent fin tops
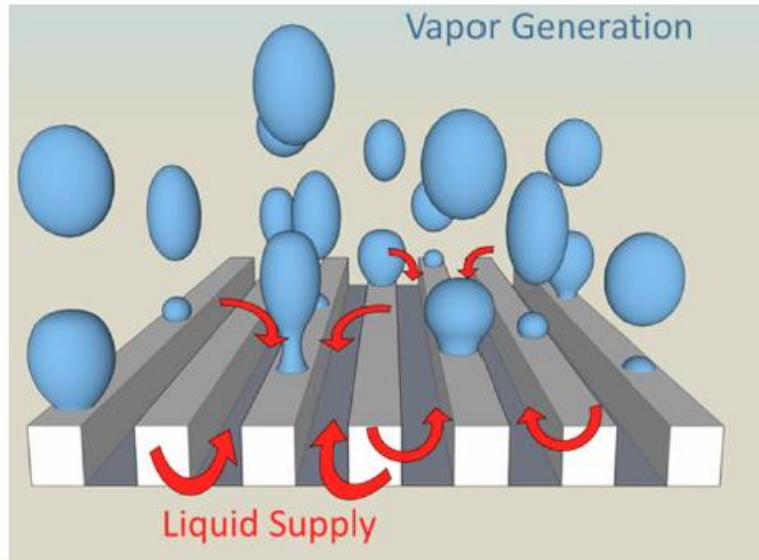
Figure 7 Proposed mechanism of bubble dynamics on microchannels by Cooke and Kandlikar[21]

Figure 7 shows the mechanism that was proposed by Cooke and Kandlikar[21] for the formation and departure of bubble. Microchannels aid in continuous supply of water to the nucleation sites that prevent the drying out of surface even with generation of large amount of vapor. Continuous supply of water in microchannels allow nucleation sites to be flooded with water leading to efficient surface re-wetting. Constant contact of water with microchannel surfaces ensures minimum wall superheat which results in high HTC. Furthermore, they also investigated the effect of notches and offset strip. These configurations resulted in poor performance which further confirmed that microchannels act as liquid conduits.

The effect of channel width, channel depth and fin width was later explained by Cooke and Kandlikar[22] in another publication. Ten chips with different parameters were tested for pool boiling performance on same setup used by Cooke and Kandlikar[21]. It was seen that with the increase in depth of microchannels, the boiling performance of the system increased. Higher depth of microchannels increased the proximity of channel

surface to the heater surface which allowed higher heat transfer. The diameter of bubble is dependent on the channel width. The bubble diameter at departure increased with increase in channel width which led to better heat transfer performance.

2.2 Microchannels Over Cylindrical Surface

Recently, a two-part experimental study of pool boiling over cylindrical microchannels test surfaces with water at atmospheric pressure was conducted by Mehta and Kandlikar[23,24]. An array of axially and circumferentially oriented microchannels over cylindrical surfaces as shown in figure 8, were tested with water at saturated condition. Heat transfer performance of the system was affected by microchannels orientation, microchannel dimensions and tube orientation.

(a) (b)
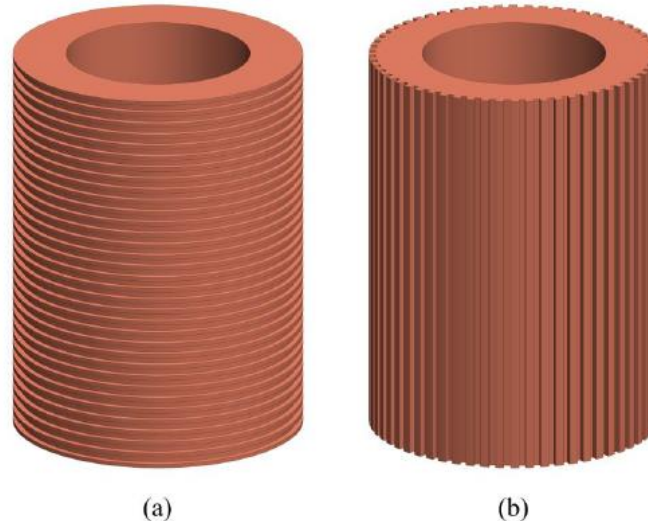
Figure 8 Schematic showing (a) CRM and (b) ARM by Mehta and Kandlikar[23,24]

The plain test section reached critical heat flux at 667 kW/m^2 with wall superheat of 17.8 K. All the microchannels were tested upto 1100 kW/m^2 without reaching critical heat flux. The improvement factor of 1.6 was obtained compared to plain section. Circumferentially

Rectangular Microchannels (CRM) yielded good results in horizontal orientation. Figure 9 shows pool boiling curve of CRM in horizontal orientation by Mehta and Kandlikar[23] with heat flux (kW/m²) on Y-axis and wall superheat (K) on X-axis.
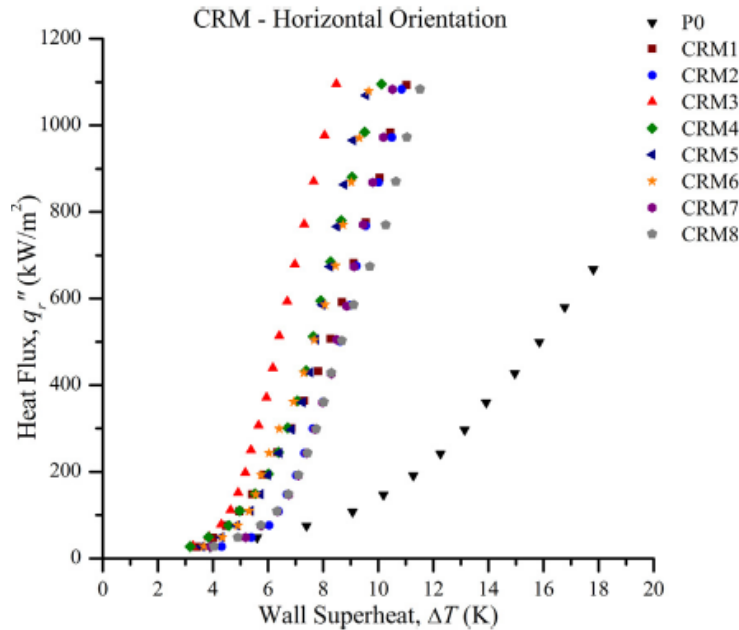
Figure 9 Pool boiling curves for CRM sections in horizontal orientation by Mehta and Kandlikar[23]

Significant enhancement in heat transfer performance was achieved with CRM in horizontal orientation. At high heat flux an enhancement factor of 2.5-3.4 was obtained. Best results were obtained for CRM 3 with heat transfer coefficient of 129 kW/m².K and wall superheat of 8.5 K at heat flux of 1095 kW/m². The bubble inside the microchannels is ejected rapidly which clears the groove area thus allowing the liquid to enter that space. The microchannels in rectangular shape were helpful for letting water to enter the microchannels and thus allowing the surface to rewet and this was responsible for lowering wall superheat and increasing the critical heat flux limits. Figure 10 shows pool boiling curve of Axially Rectangular Microchannels (ARM) in vertical orientation by Mehta and Kandlikar[24] with heat flux (kW/m²) on Y-axis and wall superheat (K) on X-axis.
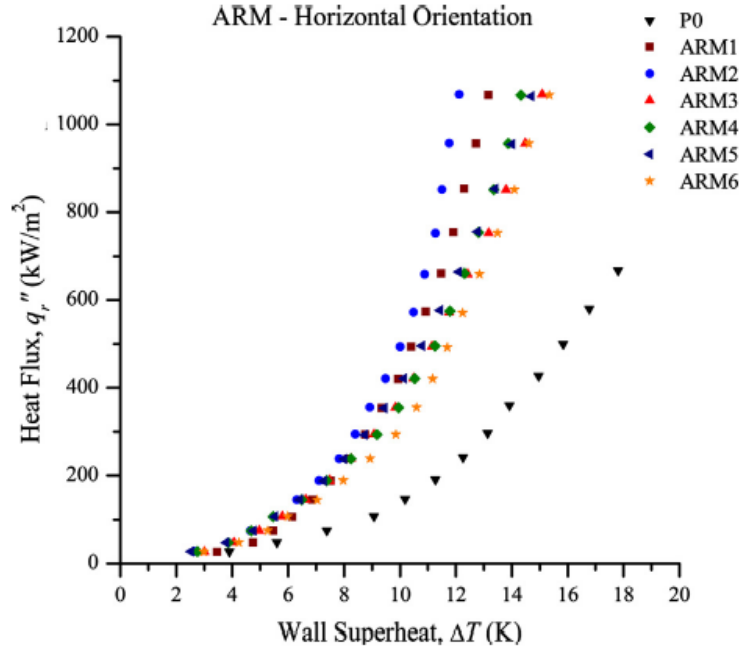
Figure 10 Pool boiling curves for ARM sections in vertical orientation by Mehta and Kandlikar[24]

The plain test section reached critical heat flux at 667 kW/m² with wall superheat of 18.8 K in vertical orientation. Significant improvement in heat transfer performance was achieved with ARM in vertical orientation. Highest result was obtained for ARM 3 with heat transfer coefficient of 96 kW/m².K and wall superheat of 11.1 K at heat flux of 1069 kW/m².

2.3 Effect of feeder channels

In 2016 Jaikumar and Kandlikar[26] explored separate liquid vapor pathways as a means of heat transfer enhancement. They used feeder channels to provide continuous supply of liquid to the nucleating regions. The bubble nucleation was confined to the nucleating regions, as the convective current of returning fluid through the feeder channels suppressed any undesirable nucleation in them. They tested four different configurations with varying length of feeder channels and the nucleating region was kept constant with

0.5 mm width. The varying length of the feeder channels were based on the bubble departure diameter for pool boiling of water on copper surface. This bubble departure diameter was very crucial to avoid the lateral coalescence and thus delay the onset of CHF leading to increased heat transfer performance. For this case the bubble departure diameter calculated was 2.123 mm, hence the feeder channels were made with various lengths close to departure diameter as shown in figure 11.
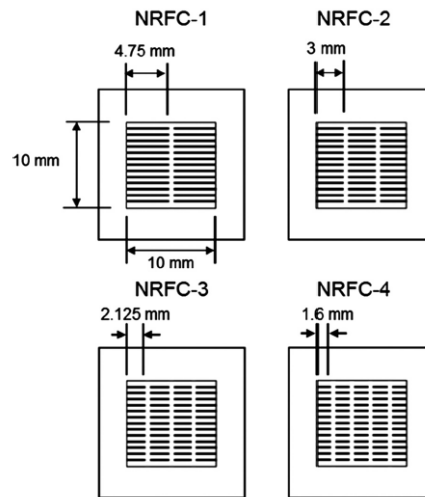
Figure 11 Test chips used by Jaikumar and Kandlikar[26]

All the chips were tested and results are presented in pool boiling curve as shown in figure 12. To serve as comparison for enhancement, plain chip was tested along with the remaining chips. The plot shows Heat flux in W/cm^2 corresponding to wall superheat in ^{o}C. While the plain chip reached CHF at 128 W/cm^2 with wall superheat of 20°C, the best performing chip (NRFC-3) reached CHF at 394 W/cm^2 at wall superheat of 5.5 ^{o}C which had the feeder channels spacing approximately equal to the bubble departure diameter.
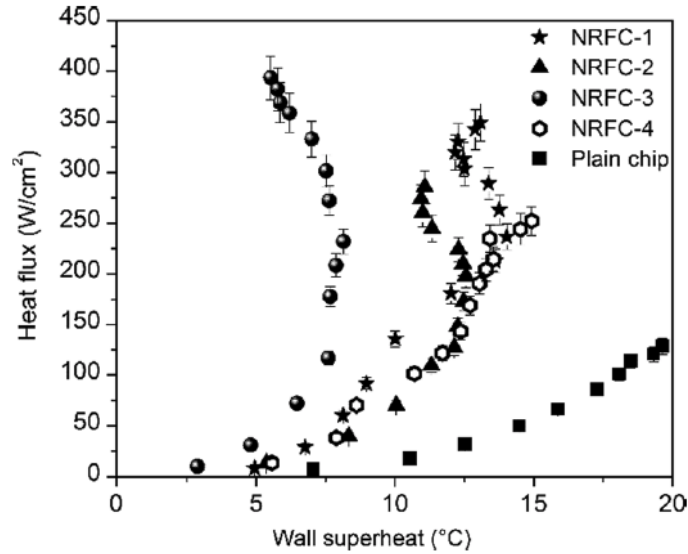
Figure 12 Pool boiling curves for the NRFC surfaces by Jaikumar and Kandlikar[26]

2.4 Enhancement through contact line augmentation

Increasing heat transfer performance of the system by using contact line region was studied by Raghupathi and Kandlikar[27]. Contact line region has higher heat flux so they tried to increase the contact line length as a means for increasing the heat transfer performance of the system. Two main sources were identified for increasing the contact line length. The first one was the surface roughness but its contribution was insignificant for improving the contact line length. Whereas contact line regions formed under the bubble growing over shallow microchannels acted as a crucial means for increasing the heat transfer. To check the effect of shallow grooves as compared to deep grooves, they tested microchannels of shallow grooves such as 10, 20 μm and deep grooves of 100 μm with varying groove width from 100 μm to 500 μm. The CHF (wetted area) vs groove width for the grooves as shown in figure 13 has two different trends.
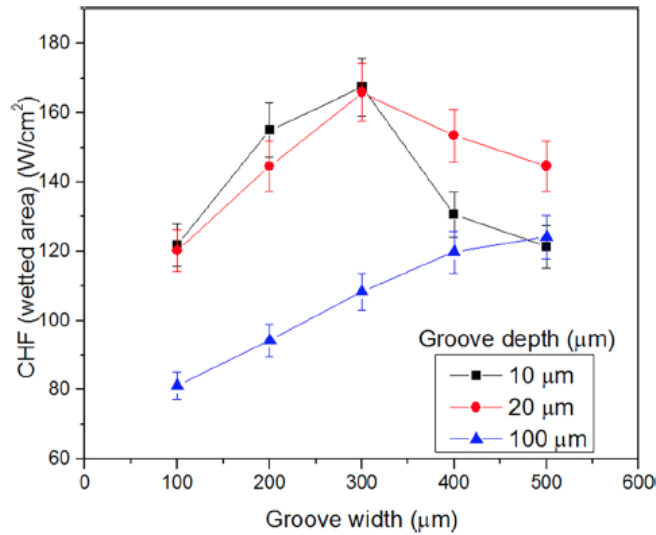
Figure 13 CHF (wetted area) vs groove width for the grooves tested by Raghupathi and Kandlikar[27]

The heat transfer performance increases as the groove width increases for shallow grooves. The heat transfer performance yielded a maximum of 187 W/cm^2 for a groove width of 300 μm and a groove depth of 20 μm. While the heat transfer performance of the 100 μm deep grooves seem to increase with increase in groove width. The maximum CHF of 124 W/cm^2 was obtained for 500 μm wide grooves, which is less than the plain surface CHF value. Specific enhancement mechanisms active for two different trends were identified using high speed imaging. It was seen that the bubble grows over multiple grooves in case of 10 and 20 μm groove depths which creates additional contact lines under the bubble base thus increasing the heat transfer performance. The growth of bubble is confined inside the walls of grooves with 100 μm depths which leads to decrease in performance.

2.5 Heat transfer enhancement by Evaporation Momentum Force (EMF)

Evaporation momentum force is experienced by the growing bubble at its interface due to difference in densities of liquid and vapor. This was used by Kandlikar[28] to increase the heat transfer performance.
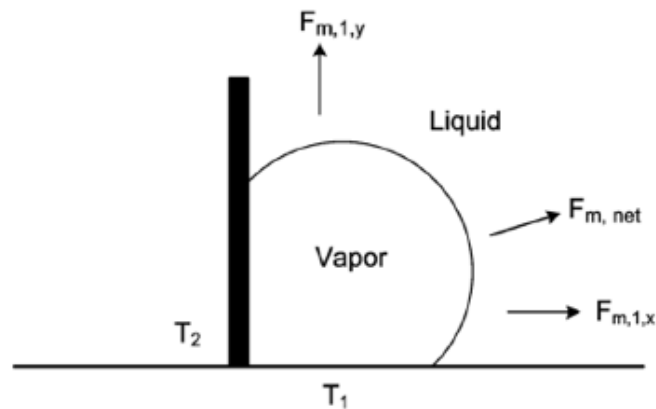
Figure 14 Schematic showing evaporation momentum force experienced by a bubble growing in a corner at fin base by Kandlikar[28]

Figure 14 shows a bubble nucleating at the corner of fin base by Kandlikar. The growing bubble experiences two EMF in two directions $X(F_{m,1,x})$ and Y $(F_{m,1,y})$. The force opposite to $F_{m,1,x}$ is absent due to presence of fin. Hence, the bubble trajectory will be resultant of these two forces in X and Y direction. If the two forces are equal then the trajectory of the bubble will be at $45°$. He assumed that there will be 50 percent less evaporation rate from the top interface. Thus, the bubble will experience higher EMF away from the Fin and the bubble trajectory will be at $14.1°$ as shown in figure 15.
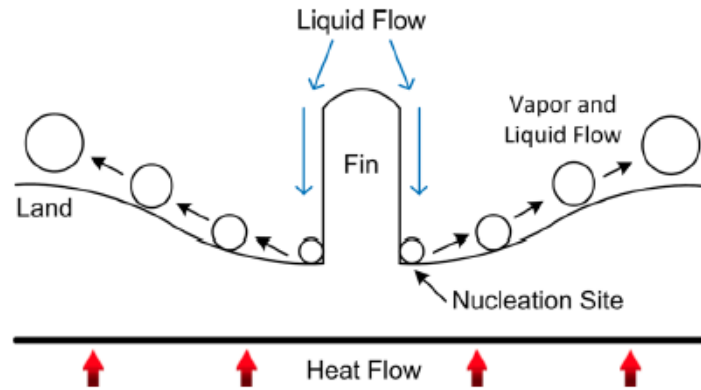
Figure 15 Enhanced surface design using evaporation momentum force to control bubble trajectory by Kandlikar[28]

Figure 15 show a schematic by Kandlikar of fin attached to heater surface. A similar structure with small fin attached to the heater surface was manufactured. The sharp corner at fin base allowed nucleation. Due to EMF, the bubbles nucleating at the bottom of the fin surface moved away from the fin surface and allowed bulk liquid to flow over fins towards nucleation sites. This facilitated the separate liquid vapor pathway thereby increasing performance to 3 MW/m^2 over plain copper surface with water as working fluid.

3.0 Experimental setup

A test setup similar to work presented by Mehta[29] was used in this experimental study. Additionally, the test setup was modified by including a CHF auxiliary loop to prevent continuous damaging of heaters after each experiment and another setup was designed to facilitate axial visualization.

3.1 Modified Setup with CHF loop

The test section assembly was mounted on a central aluminum block. This central block was held in its place by compressing it against 200 mm x 200 mm aluminum plates and borosilicate glass. 9.5 mm thick high temperature borosilicate glass was used to allow visualization while withstanding high temperatures. Silicone gaskets were used along with borosilicate to ensure leak free setup. The complete test setup as shown in figure 16 and was held using aluminum plates and M10 fasteners.
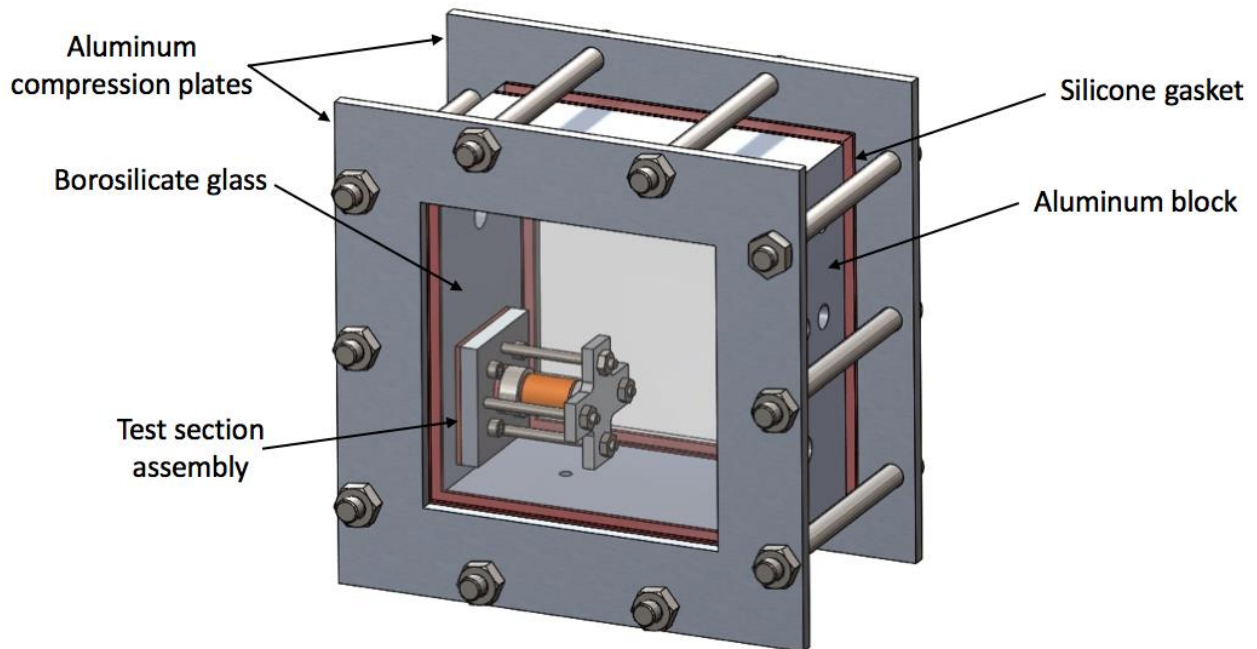
Figure 16 CAD model of assembled test setup

33

The test section assembly as shown in figure 17 consisted of primary heater which was the main source of power. The heated length of the primary heater was 19 mm hence the tubular test section was made 20 mm long. The inside diameter of test surface was 9.53 mm to closely match the outer diameter of primary heater. The axial heat loss from either side of test surface was minimized by using ceramic insulations. Silicone gaskets were used to ensure leak free setup from the test section assembly.
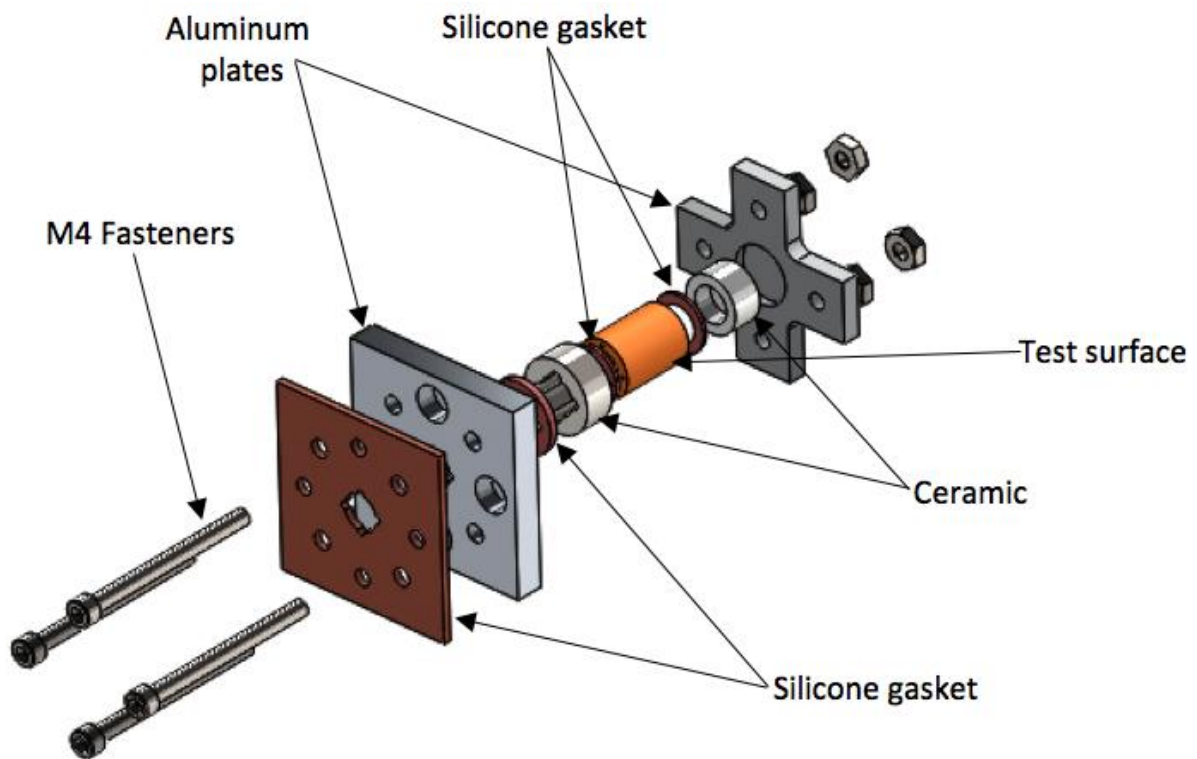
Figure 17 Test section assembly

The test section assembly was mounted on the central block by using bottom plate and fasteners. The complete test section assembly was held by compressing it laterally in between bottom plate and top plate with M4 fasteners. Thermal paste was used in

between heater and test section for ensuring high heat transfer with minimal loss in between the two.

CHF loop

A hole was manufactured in the bottom plate exactly below the test section surface to allow cold water jet to hit the test section for mitigating high temperatures formed on test section due the encapsulation of vapor around it. Pressurized cold water was stored in the container. The connection from pressurized water container to test setup was made through solenoid valve. This solenoid vale was controlled by sensor which in turn was controlled by NI Labview on the computer. So, when CHF was reached, signal through NI Labview and sensor opened the solenoid valve thus allowing the pressurized cold water to hit the test section. This breaks the vapor blanket over the test section thereby reducing the temperature.

3.2 Test surfaces

Test Chips were made of copper alloy 101. Typically, a plain test section with no surface enhancement was 20 mm long and had outer diameter of 15 mm as shown in figure 18. The inner diameter of the test section was 9.5 mm to match the outer diameter of primary heater. Four equally spaced radial holes of 1 mm diameter were made in the test section for measuring temperature using thermocouples. The holes were made at 6 mm radius from the center of cylinder and 10 mm deep.
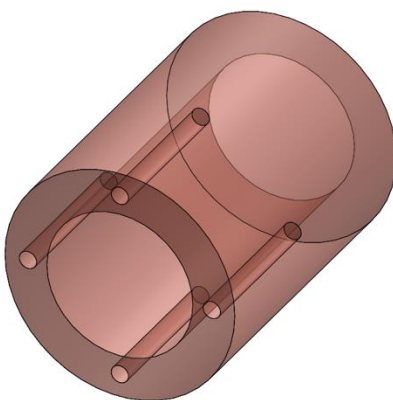
Figure 18 Cad model of plain test surface

Further surface enhancements are made on surface of the plain chip. 12 different chips with circumferentially rectangular microchannels as shown in figure 19 were machined with different parameters.
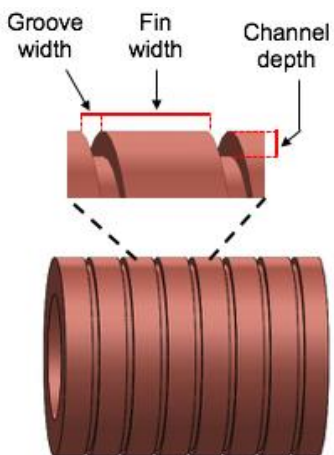
Figure 19 Schematic of CRM chip showing all parameters

The test matrix with surface enhancement parameters is given in the following table,

Table 1 Test matrix with different parameters for CRM

Chip	Fin spacing	Fin Height	Fin width
CRM 01	200 µm	50 µm	50 µm
CRM 02	200 µm	100 µm	50 µm
CRM 03	200 µm	200 µm	50 µm
CRM 04	300 µm	50 µm	50 µm
CRM 05	300 µm	100 µm	50 µm
CRM 06	300 µm	200 µm	50 µm
CRM 07	400 µm	50 µm	50 µm
CRM 08	400 µm	100 µm	50 µm
CRM 09	400 µm	200 µm	50 µm

3.3 Data reduction

A program in NI LabView was used to display the real-time temperatures and control the input voltage to the system. The program displayed temperatures from four thermocouples inserted halfway circumferentially in the test section. The fifth thermocouple inserted in water recorded bulk temperature of water. Thermocouples were spaced radially 6 mm apart with depth of 10 mm inside test section. K type thermocouples were used for measuring temperatures. Two power sources (TDK-Lambda, USA) were used to supply power to the main and auxiliary heaters. Primary heater was used to heat the test section while auxiliary heater was used to heat the water and maintain it at saturation temperature.

The heat supplied to the test section was controlled by voltage, V. The current (I) varies accordingly. The total heat supplied to the section was given by,

$$Heat\ Input,\ q_h = V \times I \tag{1}$$

To minimize the axial heat loss ceramic spacers were used on both sides of the test section.

The total heat input in radial direction was given by,

$$q_r = q_h - q_{a,l} \tag{2}$$

The axial heat loss was evaluated using 1D conduction. All the heat loss analysis and equations are given in Heat loss: Appendix

The surface area at outer diameter of the test section was given by,

$$A_s = 2\pi r_2 L \tag{3}$$

Here, r_2 is the outer radius of test section and L is length of the test section.

$$L = 20 \times 10^{-3} m \quad and \quad r_2 = 7.5 \times 10^{-3} m$$

Hence total heat flux on the area was given by,

$$Radial\ heat\ flux,\ q_r'' = \frac{q_r}{A_s} \tag{4}$$

Four thermocouples were placed circumferentially at radius r_1 (6mm), the average temperature of those thermocouples was,

$$T_{avg} = \frac{T_1 + T_2 + T_3 + T_4}{4} \tag{5}$$

The temperature at the outer surface of cylinder was calculated by using one dimensional radial conduction equation along with average temperature (T_{avg}) of all thermocouples placed at radius (r_1) and radial heat input(q_r). The surface temperature at radius r_2 was,

$$Surface\ Temperature,\ T_S = T_{ave} - \left(q_r \times \frac{ln\frac{r_2}{r_1}}{2\pi kL} \right) \tag{6}$$

where,

$$k = 400\,\frac{W}{m.K} \quad and \quad r_1 = 6 \times 10^{-3}m$$

The temperature of water was recorded by thermocouple T5 which was used to ensure water was maintained at saturated condition and to evaluate the heat transfer coefficient. The heat transfer coefficient was given by,

$$h = \frac{q_r''}{(T_S - T_5)} \tag{7}$$

3.4 Experimental procedure

The detailed procedure for conducting complete experiment is described in this section. First test section assembly was assembled along with thermocouples inserted halfway into the section. Then complete setup was assembled and all the connections were done with primary, secondary power source. All thermocouples were connected to DAQ devices and CHF loop was connected to bottom of aluminum plate. Later distilled water was filled in the test setup and it was inspected for any leaks. The test set up was taken apart and reassembled in case of leakage.

 Once the setup was checked for leaks, the secondary heater was switched on for heating water to saturation temperature. Primary heater was started once saturation condition was attained. The Input voltage to the test section was controlled by LabView program in computer. Current was obtained corresponding to applied voltage. The heat input was set in the system and it was maintained till steady state conditions were achieved in the system. Data was recorded after steady state was achieved by LabView for a span of 10

seconds at the rate of 5 Hz. After the data was logged, voltage was increased in predetermined steps of increment for recording the increase in temperatures with respect to radial heat flux. The increment in voltage was reduced near the CHF condition to obtain as many data points at higher heat fluxes as possible. The surface temperature shot up to 300 °C to 400 °C as soon as the system reached CHF.

The CHF loop was engaged as soon as the CHF condition was reached and the primary heater was turned off so as to avoid any damage to the heater or test setup. On engaging the CHF loop, solenoid valve opened up and pressurized water from the vessel which hit like a jet on the bottom surface of the chip, instantaneously reducing the surface temperature. Once the surface temperature of test chip reduced below 150 °C, CHF loop was disengaged and pressurized water jet was stopped.

After the test was over and setup was cold enough to be handled, all the water was drained. The test setup was disassembled and the test chip was taken out. This was done to prevent the oxidation of test surface in case the chip was needed to be reused.

3.5 Uncertainty analysis

All the conducted experiments are bound to have some errors in the measured parameters. These errors in measured parameter are considered by uncertainty analysis of the experiment. Uncertainty calculation for all important parameters for all tests are derived and presented in this section.

The general formula for calculating uncertainty analysis is given below,

$$U_p = \sqrt{\sum_{i=1}^{n} \left(\frac{\partial p}{\partial a_i} u_{a_i} \right)^2} \qquad (8)$$

Uncertainty in important parameters like surface temperature, radial heat flux and heat transfer coefficient are evaluated by using following formulae. The uncertainty in surface temperature is derived using equation (6) and equation (8). It is given by,

$$U_{T_s} =$$

$$\sqrt{(U_{T_{avg}})^2 + \left[\frac{\ln\frac{r_2}{r_1}}{2\pi LK}\right]^2 (U_{q_r})^2 + \left[\frac{q_r}{2\pi LKr_2}\right]^2 (U_{r_2})^2 + \left[\frac{q_r}{2\pi LKr_1}\right]^2 (U_{r_1})^2 + \left[\frac{q_r \ln\frac{r_2}{r_1}}{2\pi LK^2}\right]^2 (U_K)^2 + \left[\frac{q_r \ln\frac{r_2}{r_1}}{2\pi KL^2}\right]^2 (U_L)^2}$$

(9)

The parameters responsible for uncertainty in radial heat flux were heat input and surface area of tube. Hence after considering these two parameters, the total uncertainty in radial heat flux was derived using equation (4) and equation (8). The axial heat loss in test surface is very less compared to the heat input and thus the uncertainty associated with it is even less and hence it was neglected in calculating uncertainty for radial heat flux. Uncertainty in radial heat flux is given by equation,

$$U_{q_r''} = \sqrt{\left(\frac{1}{2\pi Lr_2}\right)^2 (U_{q_r})^2 + \left[\frac{q_r}{2\pi Lr_2^2}\right]^2 (U_{r_2})^2 + \left[\frac{q_r}{2\pi L^2 r_2}\right]^2 (U_L)^2}$$

(10)

The uncertainty in heat transfer coefficient was derived using equation (7) and equation (8). It is given by,

$$U_h = \sqrt{\left[\frac{1}{T_s - T_5}\right]^2 (U_{q_r''})^2 + \left[\frac{q_r''}{(T_s - T_5)^2}\right]^2 (U_{T_s})^2 + \left[\frac{q_r''}{(T_s - T_5)^2}\right]^2 (U_{T_5})^2}$$

(11)

The uncertainty calculations show that as the heat flux is increased, uncertainties in radial heat flux as well as heat transfer coefficient decreases and all are in acceptable range with less than 5% uncertainty.

4.0 Results and Discussion

Heat transfer enhancement on tubular surfaces was studied by two distinctive methods. Pool boiling results of both these enhancements are provided in this section. Enhancement is studied using Microgrooves on cylindrical surfaces and preferential placement of fin.

To establish a baseline and quantify the enhancement for all the surface enhanced test chips, a plain test chip was tested and all the results were compared with the plain chip results. The plain test surface achieved Critical heat flux at 68 W/cm^2 with wall superheat of 17 ^{o}C. This translated to a heat transfer coefficient of 40 kW/m^{2}K.

4.1 Enhancement by bubble diverter

CHF is initiated due to coalescence of bubbles and thus forming a continuous vapor film over the heater surface. Using the temperature data during the initiation of CHF, the temperature variation of all thermocouples was obtained. Figure 20 shows the temperature variation of all thermocouples during CHF.
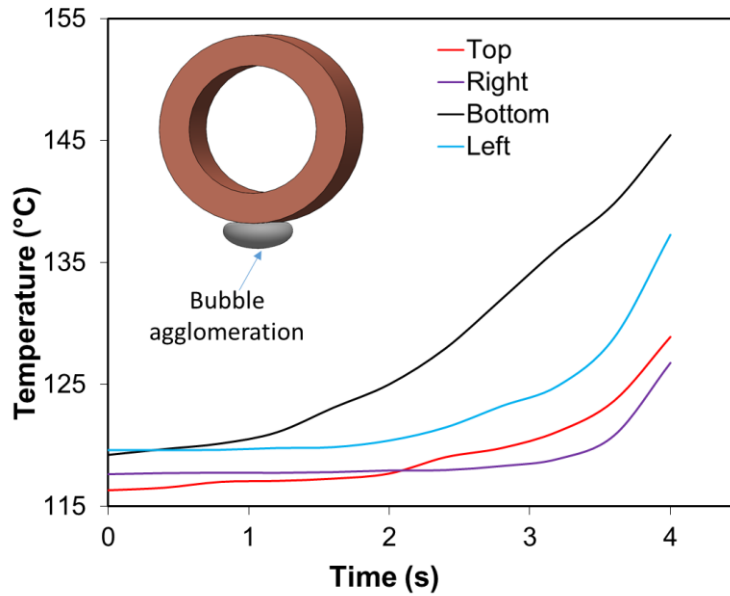
Figure 20 Temperature variation along the circumference of tube at onset of CHF by Raghupathi et al.[30]

The temperature of bottom and left thermocouple was consistently high than remaining two thermocouples. CHF was initiated from bottom thermocouple and so it spiked first. The vapor layer was first formed at bottom of cylinder and then it propagated to other parts of cylinder. Left thermocouple spiked next followed by Top and Right thermocouple after 2-3 secs. The bubble nucleating on the top or the side of cylindrical surface was taken away from the surface due to buoyancy force acting. However, the bubble nucleating on the bottom of the cylindrical tube stayed there for longer period which created local dry out and thus lead to CHF.

To increase the heat transfer performance of the system, it was necessary to delay the onset of CHF. Hence, it was necessary to deflect the bubbles nucleating from the bottom surface. So, a fin as shown in figure 21 was strategically placed at the bottom of the cylinder to avoid local dry out.
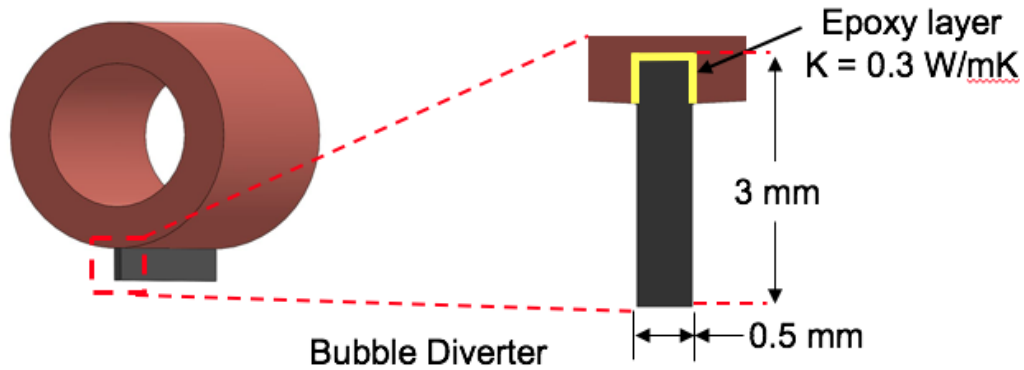
Figure 21 Schematic of Bubble Diverter

The Fin was placed in the cylinder by making a slot at the bottom surface and sticking it in the slot with epoxy. The fin was called as bubble diverter. The pool boiling curve of the bubble diverter along with plain cylindrical surface is shown in the figure 22.
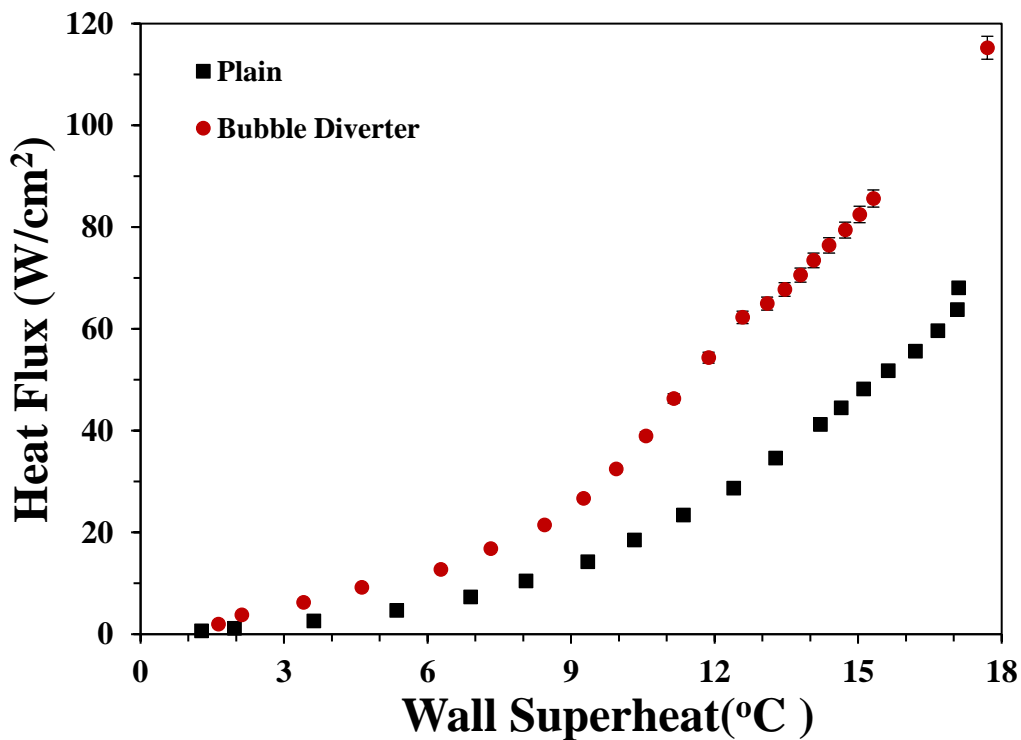
Figure 22 Pool boiling curve for bubble diverter compared to plain surface

The pool boiling curve for bubble diverter and pain surface shows the radial heat flux on Y axis in W/cm^2 and the wall superheat on X axis in ^{o}C. The CHF for plain chip is 68

W/cm^2 at 17 ^{o}C. The bubble diverter showed an enhancement of 60% attaining a CHF at 115 W/cm^2 at 18 ^{o}C of wall superheat.

This enhancement was seen in heat transfer coefficient as well as for bubble diverter. Figure 23 shows the graph of heat transfer coefficient in kW/m^2^{o}C vs radial heat flux in W/cm^2.
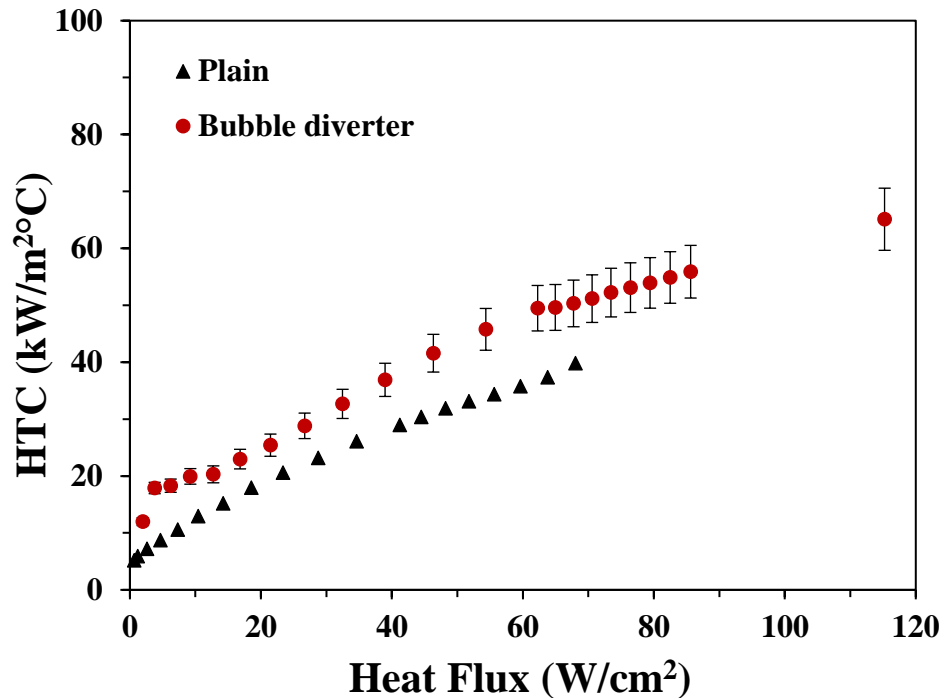
Figure 23 Heat flux vs Heat transfer coefficient for bubble diverter compared to plain surface

Bubble diverter achieved a heat transfer coefficient of 65 kW/m^{2}K as compared to 40 kW/m^{2}K for plain chip. Thus, the addition of single bubble diverter at the bottom of the plain chip gave an enhancement of 65% in radial heat flux and 75% in heat transfer coefficient.

Evaporation momentum force (EMF), is a reactionary force experienced at the bubble interface due to the sudden expansion of the evaporating mass[30]. The addition of bubble fin diverter explored EMF on the bubble nucleating on the bottom surface thus

modulating the flow field in that area. The fin is at lower temperature than the cylindrical surface and the epoxy layer being a poor conductor adds to that. Hence the bubble nucleating on the base of fin experienced higher EMF away from the fin surface. Thus, the nucleating bubble was displaced away from the fin surface making room for water to rewet the surface. This lead to separate liquid vapor pathway ensuring continuous rewetting of surface and thus avoiding local dry out. The general equation for the net EMF[30] is given by,

$$F_M = \int \eta^2 (\rho_v^{-1} - \rho_l^{-1}) dA$$

Where,

$$\eta \ is \ local \ mass \ flux$$

$$\rho_v \ is \ vapor \ density \ and \ \ \rho_l \ is \ liquid \ density$$

The variation of mass flux across interface and EMF experienced by the bubble was evaluated similar to Raghupathi and Kandlikar[31]. The EMF increases with increase in heat flux and it is very efficient at high heat flux. Figure 24 shows the ratio of EMF with buoyancy force experienced by the bubble at the base of bubble diverter by Raghupathi et al.[30]
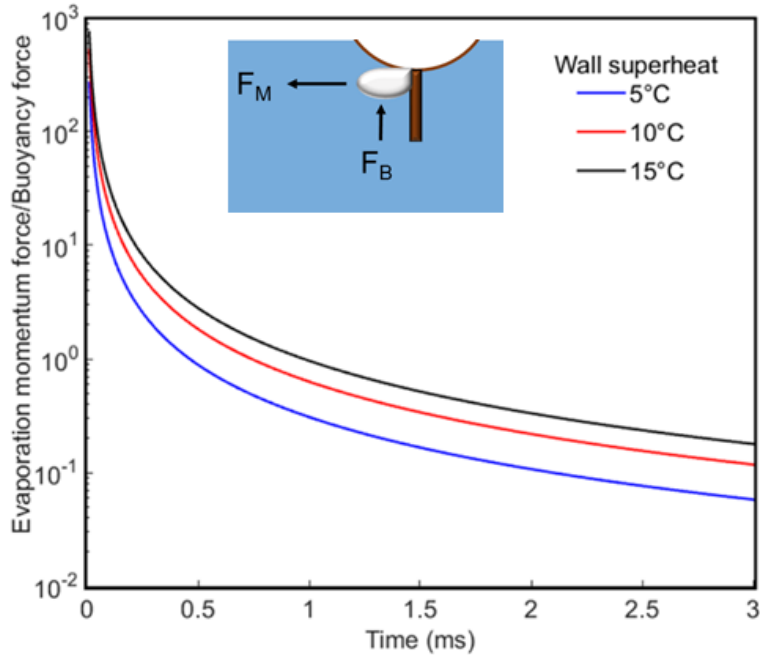
Figure 24 Ratio of EMF to buoyancy force for bubble nucleating at base of bubble diverter[30]

The figure 24 shows ratio of EMF over buoyancy force with respect to time (ms) for different degrees of wall superheat. The direction of EMF and buoyancy force acting on the bubble nucleating at the base of diverter is shown in figure 20. The EMF is higher at initial bubble growth stage and then as the bubble size increases, EMF becomes less than buoyancy force. Thus, we get high lateral displacement velocity of bubble during its initial growth stages and then eventual decrease as the bubble size increases. This lateral displacement of bubble facilitates separate liquid vapor pathway near the fin base. The quick displacement of bubble from the base of cylindrical surface is responsible for delaying CHF and increased heat transfer performance. The circumferential thermocouple data during CHF was obtained at the time of testing and it is plotted in the figure 25 shown below.
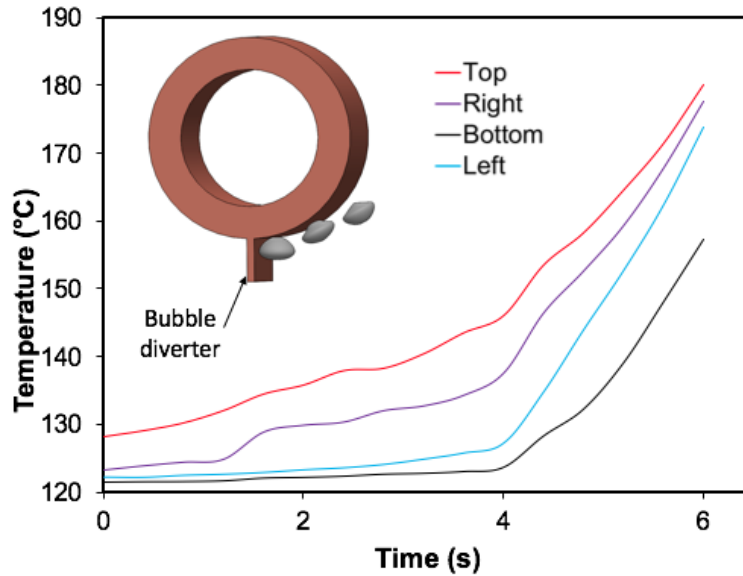
Figure 25 Temperature variation along the circumference of bubble diverter at onset of CHF by Raghupathi et al.[30]

The thermocouple temperature variation is plotted against time during CHF for the bubble fin diverter. It was seen that the top thermocouple was consistently higher than remaining thermocouples. CHF was initiated from the top thermocouple as its temperature increased tremendously. After Top thermocouple, the vapor film covered the right part of the chip and its temperature spiked, but the temperature of bottom and left thermocouple remained the same. Later the vapor film encapsulated the right side of cylinder and then at last it covered the bottom surface. This vapor propagation was completely opposite than that of the plain chip. This change in the CHF initiation and vapor propagation was due to efficient vapor removal by bubble diverter.

Figure 26 Bubble displacement captured using high speed imaging at 4000 fps by Raghupathi et al.[30]

Figure 26 shows the direction of displacement of bubble from its initiation to departure at 4-degree wall superheat. The images were captured at 4000 fps. The images are arranged in sequence 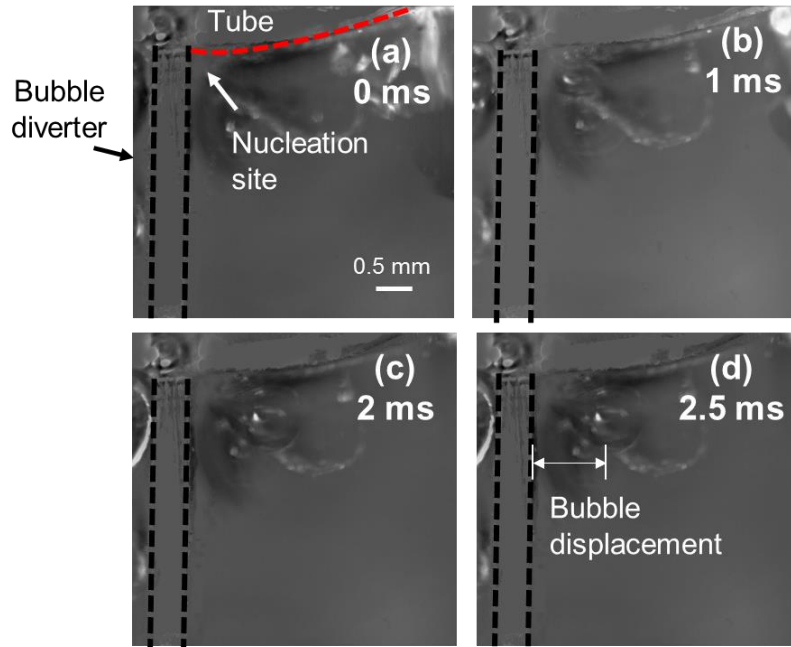from the nucleation of bubble to its departure. In figure 26 the bubble diverter is shown in black dotted lines. The tubular surface is shown in red dotted line. The bubble diverter is attached to the tubular surface using epoxy. In (a) the nucleation site of the bubble was shown at the intersection of bubble diverter and tubular surface. After 1 ms, nucleation was seen at intersection of bubble diverter and tubular surface in (b). After another 1 ms, the was bubble seen growing towards the direction of tubular surface in (c). The last frame (d) shown the completely grown bubble about to depart. The displacement of the bubble was seen away from the diverter towards the cylindrical surface. This is because the cylindrical surface is at higher temperature than bubble diverter. Hence the bubble experiences higher EMF force towards the cylindrical surface. This allows the nucleating bubble to depart easily thus ensuring continuous

rewetting of surface thereby creating separate liquid vapor pathway at the bottom of the cylinder which enhances heat transfer performance.

4.2 Effect of area enhancement and contact line

In this section, results of enhancement using various Circumferential rectangular microchannels are presented. Various chips with varying parameters were tested for studying the enhancement using microgrooves. All the test chips were designed in SolidWorks and manufactured in Machine shop lab at Rochester Institute of Technology. Different mechanisms were identified and studied by varying parameters in microgrooves. For the parametric study of different microchannels, two parameters were kept constant and only one parameter was varied. All the tested chips were grouped together according to varying groove width while keeping the groove depth and fin width constant. The table shows the group 1 of microchannels tested with varying groove width for a groove depth of 50 μm.

Table 2 Test matrix with different parameters for CRM group 1

CRM	Fin width (μm)	Groove depth (μm)	Groove width (μm)
CRM 01	50	50	200
CRM 02	50	50	300
CRM 03	50	50	400

The pool boiling curve with all the CRM compared with plain chip are shown in figure 27. The wall superheat is presented on X axis in ^{o}C while the radial heat flux for all the chips is presented on Y axis in W/cm^2.

Figure 27 Pool boiling curve for CRM group 1

It was seen that for a constant fin width of 50 μm and constant groove width of 50 μm, the chip with the narrowest channels of 200 μm performed better than remaining chips. The 200 μm chip reached CHF at a heat flux of 98 W/cm^2 with a wall superheat of 13°C. This translated to 44 percent of heat transfer enhancement. The Uncertainty evaluated at highest heat flux in 200 μm was about 2% which is in the acceptable range.

Figure 28 Heat flux vs Heat transfer coefficient for CRM group 1

Figure 28 shows the graph of heat flux in W/cm^2 vs. heat transfer coefficient in $kW/m^{2o}C$. The 200 μm chip gave a heat transfer coefficient of 77 $kW/m^{2o}C$. The heat transfer performance of any test chip is most important at the higher heat flux condition. Hence, the uncertainty in heat transfer coefficient was determined at all heat flux conditions and it was about 4.7 percent which is in acceptable range.

For the next group of chips the groove depth was increased to 100 μm while keeping remaining parameters same. The test matrix for group 2 chips are as shown below,

Table 3 Test matrix with different parameters for CRM group 2

CRM	Fin width (µm)	Groove depth (µm)	Groove width (µm)
CRM 04	50	100	200
CRM 05	50	100	300
CRM 06	50	100	400

The pool boiling curve with all the CRM compared with plain chip are shown in figure 29. The wall superheat is presented on X axis in °C while the radial heat flux for all the chips is presented on Y axis in W/cm^2.
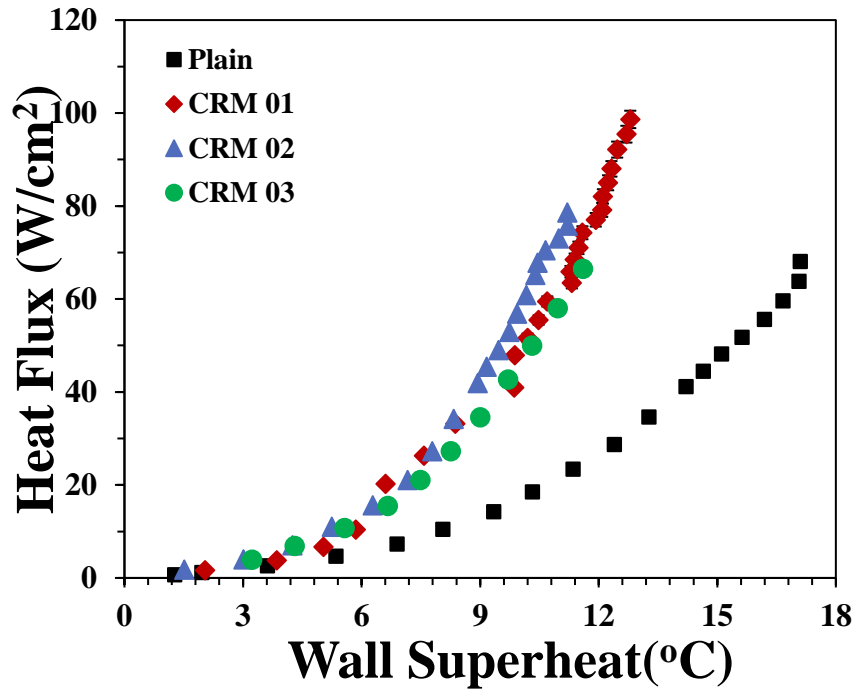

Figure 29 Pool boiling curve for CRM group 2

It was seen that similar to group 1, the chip with smallest groove width yielded highest performance. The performance went on decreasing as the groove width increased. The

200 μm chips reached CHF at 101 W/cm^2 for a wall superheat of 11 ^{o}C. The enhancement in CHF compared to plain chip was about 48 percent. Uncertainty was evaluated at all heat fluxes. An uncertainty of 4.3 percent was observed at lowest heat flux and uncertainty of 1.9 percent at highest heat flux was obtained.
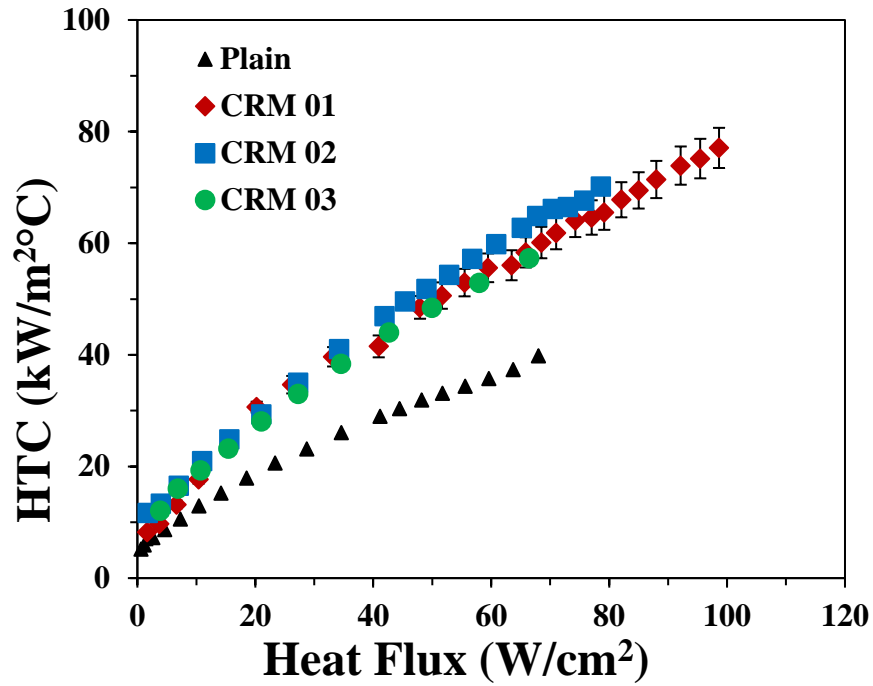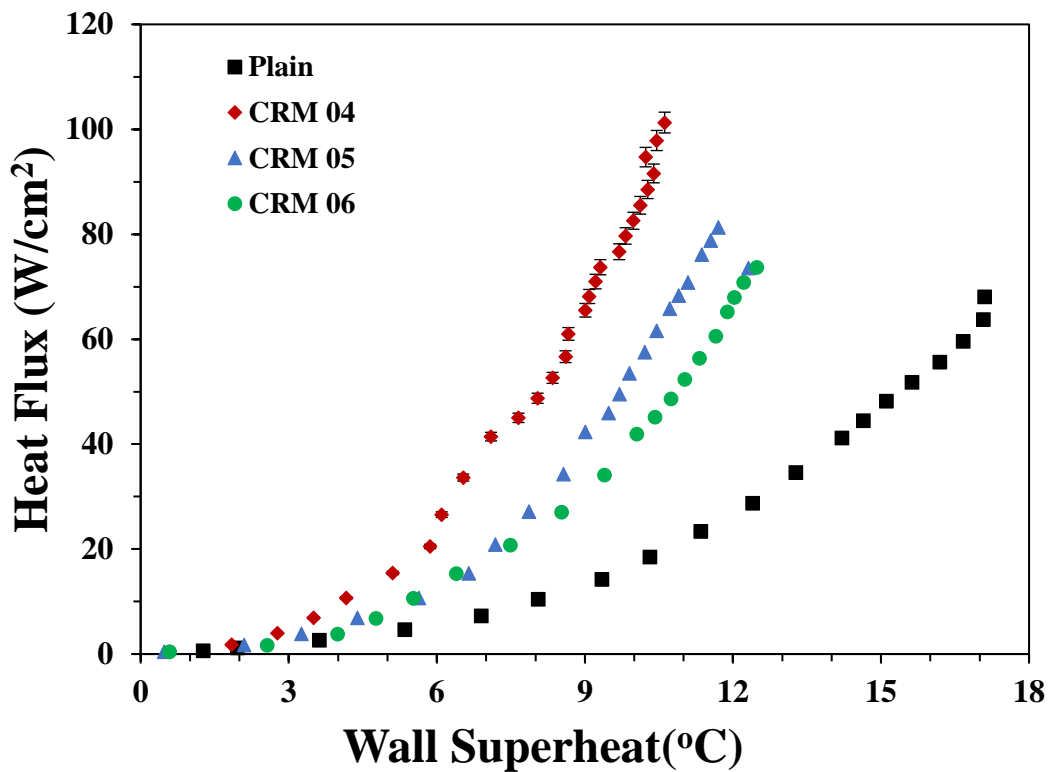

Figure 30 Heat flux vs Heat transfer coefficient for CRM group 2

Figure 30 shows the graph of heat flux in W/cm^2 to heat transfer coefficient in kW/m^{2o}C. Results similar to heat flux were observed, the chip with smallest microchannels yielded highest heat transfer coefficient. CRM 04 obtained heat transfer coefficient of 95 kW/m^{2o}C before hitting CHF for a wall superheat of 11 ^{o}C. The uncertainty in heat transfer coefficient at highest heat flux was around 4.5 percent.

Group 3 consisted of chips with 50 μm fin width, 200 μm groove depth and the groove width was varied. Table 3 shows the matrix for group 3.

CRM	Fin width (μm)	Groove depth (μm)	Groove width (μm)
CRM 07	50	200	200
CRM 08	50	200	300
CRM 09	50	200	400

All the chips in group 3 were tested till highest heat flux. The pool boiling curve for the chips is shown in figure 31. Heat flux in W/cm^2 on Y axis is plotted against wall superheat on X axis.
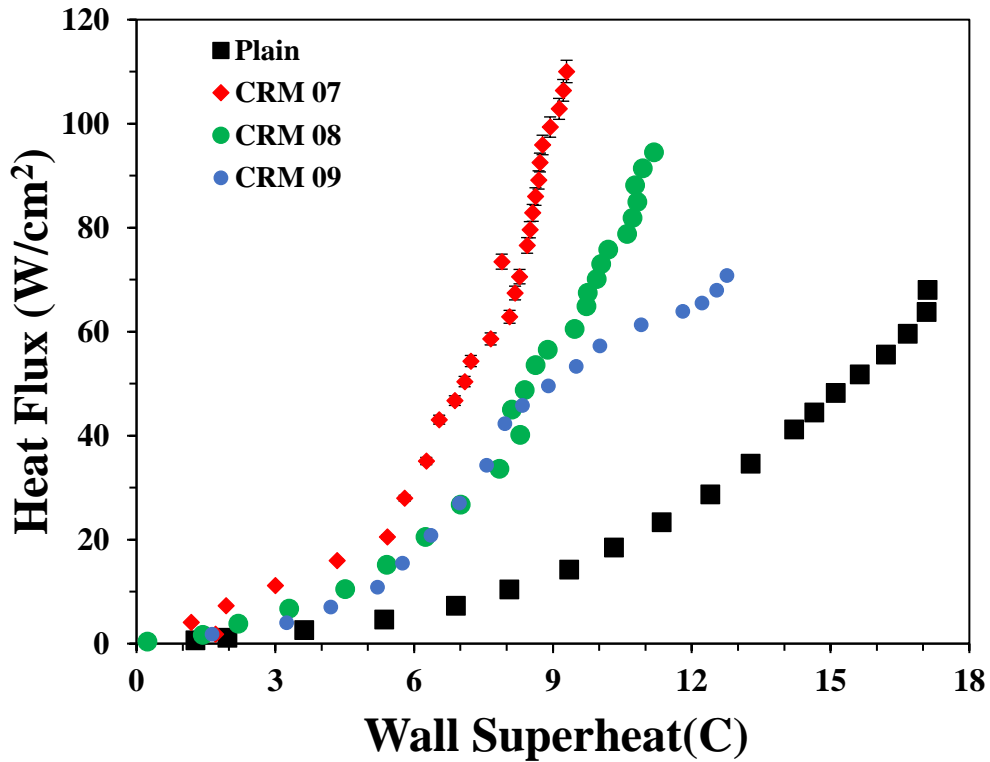
Figure 31 Pool boiling curve for CRM group 3

In group 3 for constant fin width and groove depth, it is seen that the performance increases as the groove width decreases. The best result was obtained by the chip with 200 µm groove width which is consistent with results of previous groups. The highest heat flux of 110 W/cm^2 was obtained for a wall superheat of 12 °C. The uncertainty analysis was calculated for all chips in group 3 and it was well in the accepted limits for all the chips. The uncertainty for the best performing chip, CRM 07 at lowest heat flux was 4.2 percent and at highest heat flux was 1.95 percent. Two chips, CRM 07 and CRM 09 were tested till very high heat flux but did not reach CHF.
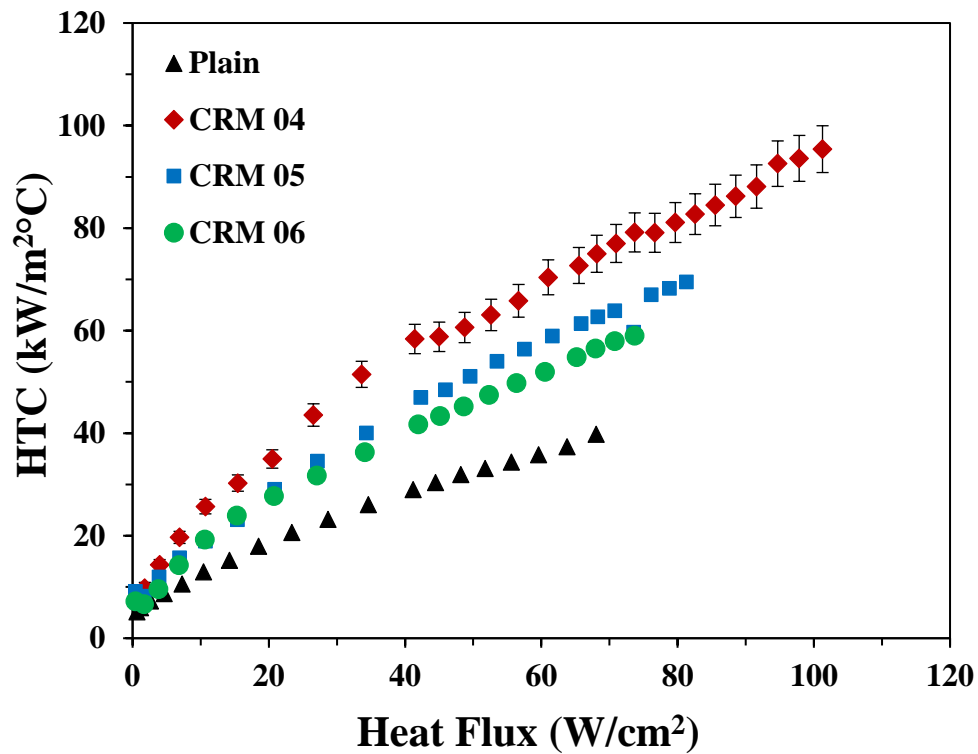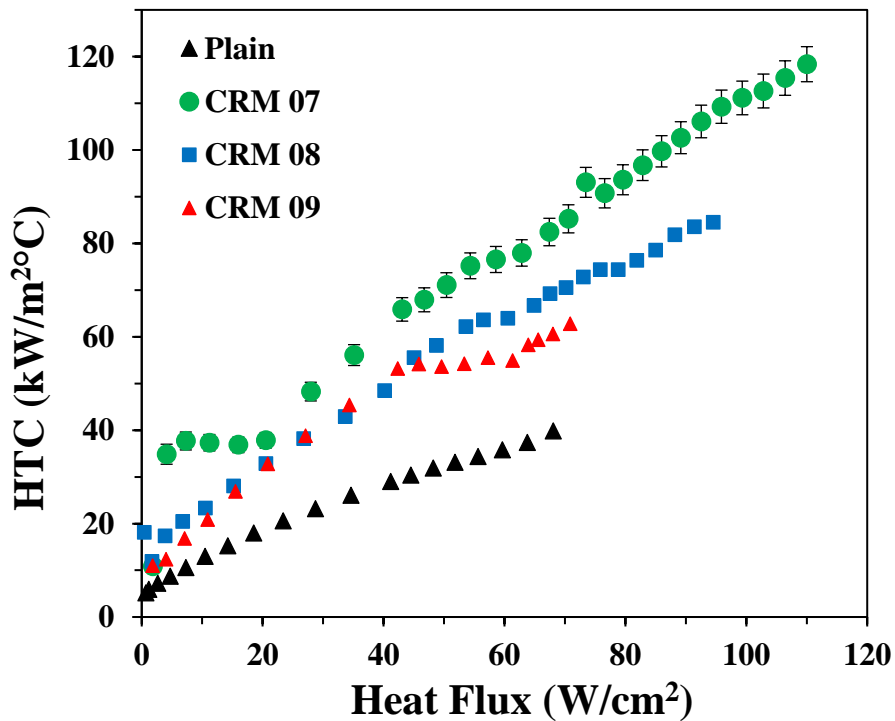

Figure 32 Heat flux vs Heat transfer coefficient for CRM group 3

Figure 32 shows the graph of heat flux vs heat transfer coefficient. The heat transfer coefficient is shown on Y axis in kW/m^2°C and heat flux is shown on X axis in W/cm^2. A heat transfer coefficient of 118 kW/m^2°C with 3 percent uncertainty at highest heat flux was obtained.

<u>Area Enhancement effect</u>

Area enhancement is the additional area available for heat transfer on the test section due to presence of microchannels. The area enhancement for test surfaces in all sections is given below,

Table 5 Area enhancement for all CRM

Group	CRM	Area enhancement
Group 1	CRM 01	1.4
	CRM 02	1.28
	CRM 03	1.2
Group 2	CRM 04	1.8
	CRM 05	1.6
	CRM 06	1.4
Group 3	CRM 07	2.6
	CRM 08	2.1
	CRM 09	1.8

The figure shows area enhancement of all test surfaces on Y axis along with increment in the groove width on X axis.

It is evident from the table 5 and figure 33 that in each group as the groove width increases the area enhancement decreases. This is because as the groove width increases the number of grooves on the surface decreases, thus decreasing the area available for heat transfer.
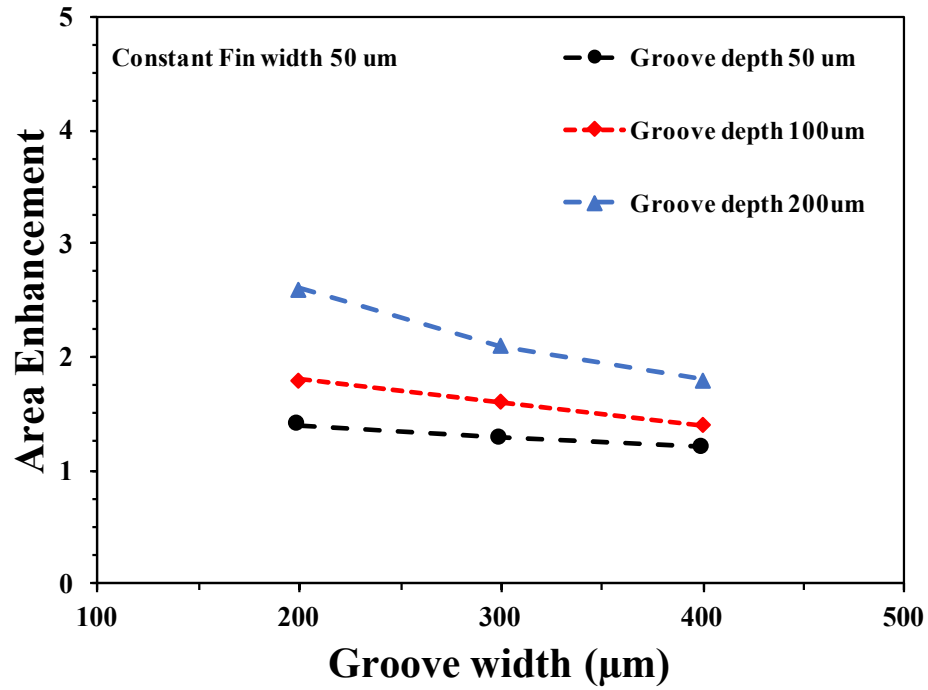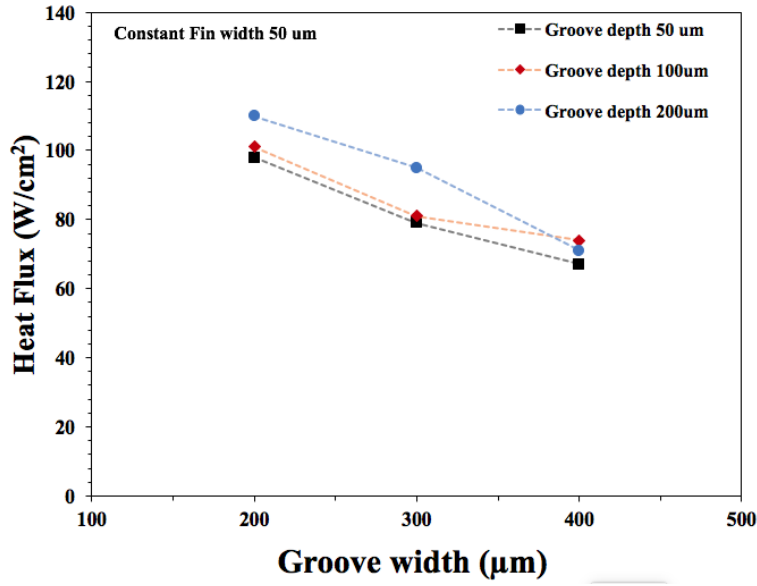
Figure 34 Highest heat flux for all CRM vs groove width for varying groove depths

Figure 30 shows highest heat flux obtained by all chips with increment in the groove width of all surfaces. As the groove width increases, the number of microchannels on the test surfaces decreases. This reduces the area enhancement on the test surface. It is seen from figure that the heat transfer performance of the test surface increases with increase in area enhancement for all groups.

Contact line Effect

It is well established in literature[27] that contact line region affects CHF of the system. Increasing contact line increases heat transfer. Contact line region has higher heat fluxes. Hence, increasing contact line region increases evaporation rate. Use of microchannels is one of the methods to increase contact line.
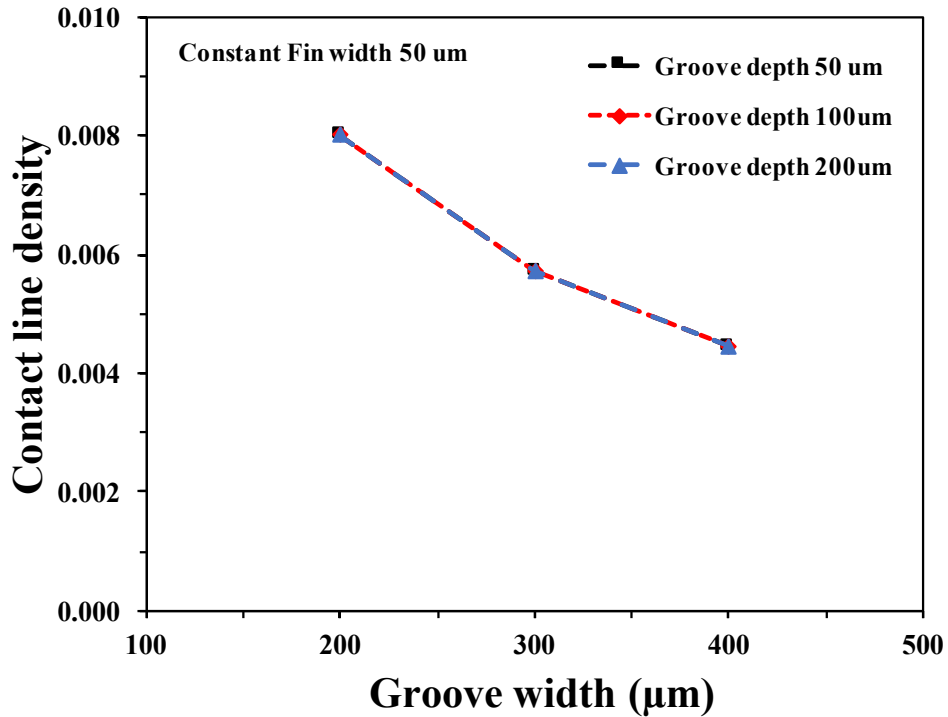
Figure 35 Effect of groove width and groove depth on contact line density

Figure 31 shows the contact line density on Y axis and groove width in X axis. It is seen that as the groove width decreases i.e. as the microchannels become narrow the contact line density increases. The contact line density increases equally for all microchannels with the increases in groove width. Figure 30 & 31 show that the heat transfer performance of the system is affected contact line density. As the contact line density increases the highest heat flux attained by the system also increases for all the groups.

5.0 Conclusions

Pool boiling of water over cylindrical surfaces with various enhancements was studied with an aim to eventually increase the heat transfer performance by pushing CHF. Plain surface was tested with water to establish a baseline performance. Various surface enhancement techniques were employed to evaluate the effect of those techniques on heat transfer performance. Following conclusions are drawn after carefully analyzing all the experimental results,

Plain surface was tested with water, it yielded CHF of 68 W/cm^2 at a wall superheat of 17 ^{o}C. A heat transfer coefficient of 40 $kW/m^{2o}C$ was obtained for plain surface at highest heat flux. Bubble diverter was used as one of the enhancement technique and it yielded a CHF of 115 W/cm^2 at a wall superheat of 18 ^{o}C with heat transfer coefficient of 65 $kW/m^{2o}C$. This translated to an enhancement of 60% in heat flux.

All the CRM were tested upto CHF. CRM 07 with 400 µm groove width and 200 µm groove depth yielded the highest performance without reaching CHF. CRM 07 yielded heat flux of 110 W/cm^2 at wall superheat of 9 ^{o}C with heat transfer coefficient of 118 $kW/m^{2o}C$. This translated to an enhancement of 62% in heat flux. In all the CRM that were tested two mechanisms dictated the increase in heat transfer performance. Increment in heat transfer can be seen due to area enhancement and increase in contact line. Portioning of heat transfer mechanisms is not possible; hence it cannot be distinguished which mechanism was responsible for increment in heat transfer.

The temperature variation during the onset of CHF for plain surface revealed that CHF initiates from the bottom of cylindrical surface. Hence a fin was added at the bottom of the cylindrical surface which resulted in substantial heat transfer performance increment.

The Bubble diverter modulated the flow around the cylinder enabling separate liquid vapor pathways.

From high speed imaging, it was evident that the nucleating bubble was displaced away from the bubble diverter towards the cylindrical surface. This ensured continuous rewetting of surface even at higher heat fluxes. The thermocouple temperature variation data during the onset of CHF for Bubble diverter revealed that CHF initiated from the top surface unlike plain surface where it originated from bottom. This could be the effect of flow modulation around the cylinder caused by the bubble diverter.

6.0 Future Work

Tubular sections are at the heart of refrigeration and air conditioning industries where refrigerants are used as cooling medium. Current work dealt with water as working fluid to identify different mechanisms affecting the performance of the system. Testing with water also allowed to quantify the results by comparing them to well established results in literature. But going forward it would be interesting to see the effects of these mechanisms with refrigerants as working medium which are directly applicable to refrigeration and air conditioning industry.

For the cylindrical surface in horizontal orientation CHF is seen to initiate from the bottom hence preferential placement of fin increased the heat transfer performance. This mechanism of flow of bubbles around cylinder would change with change in orientation. Hence, the plain surface should be studied and tested for the initiation of CHF in vertical orientation. And based on the results appropriate method should be employed for performance enhancement.

CHF initiates from top of the cylindrical surface for the chip with bubble diverter. The bubble diverter ensures separate liquid vapor pathways on the bottom but there is no enhancement on top surface which results in CHF initiation from top. It would be interesting to study the enhancement where the bubble diverter is placed on the bottom surface with some enhancement on top like porous coating or microgrooves.

References

[1] Kang, M.-G., and Han, Y.-H., 2002, "Effects of Annular Crevices on Pool Boiling Heat Transfer," Nucl. Eng. Des.

[2] Kang, M.-G., 2005, "Effects of Outer Tube Length on Saturated Pool Boiling Heat Transfer in a Vertical Annulus with Closed Bottoms," Int. J. Heat Mass Transf., **48**(13), pp. 2795–2800.

[3] Kang, M.-G., 2011, "Pool Boiling Heat Transfer in a Vertical Annulus with a Stepped Outside Tube," Int. J. Heat Mass Transf., **54**(23-24), pp. 4817–4822.

[4] Kang, M.-G., 2007, "Pool Boiling Heat Transfer on a Vertical Tube with a Partial Annulus of Closed Bottoms," Int. J. Heat Mass Transf., **50**(3-4), pp. 423–432.

[5] Kang, M.-G., 2002, "Pool Boiling Heat Transfer in Vertical Annular Crevices," Int. J. Heat Mass Transf., **45**(15), pp. 3245–3249.

[6] Kang, M.-G., 2008, "Effects of the Location of Side Inflow Holes on Pool Boiling Heat Transfer in a Vertical Annulus," Int. J. Heat Mass Transf., **51**(7-8), pp. 1707–1712.

[7] Kang, M.-G., 2010, "Pool Boiling Heat Transfer on the Tube Surface in an Inclined Annulus," Int. J. Heat Mass Transf., **53**(15-16), pp. 3326–3334.

[8] Prakash Narayan, G., Anoop, K. B., Sateesh, G., and Das, S. K., 2008, "Effect of Surface Orientation on Pool Boiling Heat Transfer of Nanoparticle Suspensions," Int. J. Multiph. Flow, **34**(2), pp. 145–160.

[9] Narayan, G. P., Anoop, K. B., and Das, S. K., 2007, "Mechanism of Enhancement/deterioration of Boiling Heat Transfer Using Stable Nanoparticle Suspensions over Vertical Tubes," J. Appl. Phys., **102**(7), p. 074317.

[10]   Das, S. K., Putra, N., and Roetzel, W., 2003, "Pool Boiling Characteristics of Nano-Fluids," Int. J. Heat Mass Transf., **46**(5), pp. 851–862.

[11]   Kole, M., and Dey, T. K., 2012, "Investigations on the Pool Boiling Heat Transfer and Critical Heat Flux of ZnO-Ethylene Glycol Nanofluids," Appl. Therm. Eng., **37**, pp. 112–119.

[12]   Trisaksri, V., and Wongwises, S., 2009, "Nucleate Pool Boiling Heat Transfer of TiO2?R141b Nanofluids," Int. J. Heat Mass Transf., **52**(5-6), pp. 1582–1588.

[13]   Naphon, P., and Thongjing, C., 2014, "Pool Boiling Heat Transfer Characteristics of Refrigerant-Nanoparticle Mixtures," Int. Commun. Heat Mass Transf., **52**, pp. 84–89.

[14]   Hegde, R. N., Rao, S. S., and Reddy, R. P., 2012, "Studies on Nanoparticle Coating due to Boiling Induced Precipitation and Its Effect on Heat Transfer Enhancement on a Vertical Cylindrical Surface," Exp. Therm. Fluid Sci., **38**, pp. 229–236.

[15]   Kulenovic, R., Mertz, R., and Groll, M., 2002, "High Speed Flow Visualization of Pool Boiling from Structured Tubular Heat Transfer Surfaces," Exp. Therm. Fluid Sci.

[16]   Ji, W.-T., Numata, M., He, Y.-L., and Tao, W.-Q., 2015, "Nucleate Pool Boiling and Filmwise Condensation Heat Transfer of R134a on the Same Horizontal Tubes," Int. J. Heat Mass Transf., **86**, pp. 744–754.

[17]   Memory, S. B., Sugiyama, D. C., and Marto, P. J., 1995, "Nucleate Pool Boiling of R-114 and R-114-Oil Mixtures from Smooth and Enhanced surfaces—I. Single Tubes," Int. J. Heat Mass Transf., **38**(8), pp. 1347–1361.

[18]   Kang, M.-G., 1999, "Effect of Tube Inclination on Pool Boiling Heat Transfer," J. Heat Transf., **122**(1), pp. 188–192.

[19]   Sateesh, G., Das, S. K., and Balakrishnan, A. R., 2009, "Experimental Studies on the Effect of Tube Inclination on Nucleate Pool Boiling," Heat Mass Transf., **45**(12), pp. 1493–1502.

[20]   Chien, L.-H., and Webb, R. L., 1998, "Visualization of Pool Boiling on Enhanced Surfaces," Exp. Therm. Fluid Sci.

[21]   Cooke, D., and Satish G. Kandlikar, 2011, "Pool Boiling Heat Transfer and Bubble Dynamics Over Plain and Enhanced Microchannels," J. Heat Transf., **133**(5), pp. 052902–052902.

[22]   Cooke, Dwight, and Kandlikar, S.G., 2012, "Effect of Open Microchannel Geometry on Pool Boiling Enhancement," Int. J. Heat Mass Transf., **55**(4), pp. 1004–1013.

[23]   Mehta, J. S., and Kandlikar, S. G., 2013, "Pool Boiling Heat Transfer Enhancement over Cylindrical Tubes with Water at Atmospheric Pressure, Part I: Experimental Results for Circumferential Rectangular Open Microchannels," Int. J. Heat Mass Transf., **64**, pp. 1205–1215.

[24]   Mehta, J. S., and Kandlikar, S. G., 2013, "Pool Boiling Heat Transfer Enhancement over Cylindrical Tubes with Water at Atmospheric Pressure, Part II: Experimental Results and Bubble Dynamics for Circumferential V-Groove and Axial Rectangular Open Microchannels," Int. J. Heat Mass Transf., **64**, pp. 1216–1225.

[25]   You, S. M., 1997, "Enhanced Boiling Heat Transfer from Micro-Porous Cylindrical Surfaces in Saturated FC-87 and R-123," J. Heat Transf., **119**, p. 319.

[26]   Jaikumar, A., and Kandlikar, S. G., 2016, "Pool Boiling Enhancement through Bubble Induced Convective Liquid Flow in Feeder Microchannels," Appl. Phys. Lett., **108**(4), p. 041604.

[27]   Raghupathi, P. A., and Kandlikar, S. G., 2017, "Pool Boiling Enhancement through Contact Line Augmentation," Appl. Phys. Lett., **110**(20), p. 204101.

[28]   Kandlikar, S. G., 2013, "Controlling Bubble Motion over Heated Surface through Evaporation Momentum Force to Enhance Pool Boiling Heat Transfer," Appl. Phys. Lett., **102**(5), p. 051611.

[29]   Jeet S. Mehta, 2013, "Enhanced Pool Boiling of Water with Open Microchannels over Cylindrical Tubes," Rochester Institute of Technology.

[30]   Raghupathi, P. A., Joshi, I. M., Jaikumar, A., Emery, T. S., and Kandlikar, S. G., 2017, "Bubble Induced Flow Field Modulation for Pool Boiling Enhancement over a Tubular Surface," Appl. Phys. Lett., **110**(25), p. 251603.

[31]   Raghupathi, P. A., and Kandlikar, S. G., 2016, "Bubble Growth and Departure Trajectory under Asymmetric Temperature Conditions," Int. J. Heat Mass Transf., **95**, pp. 824–832.
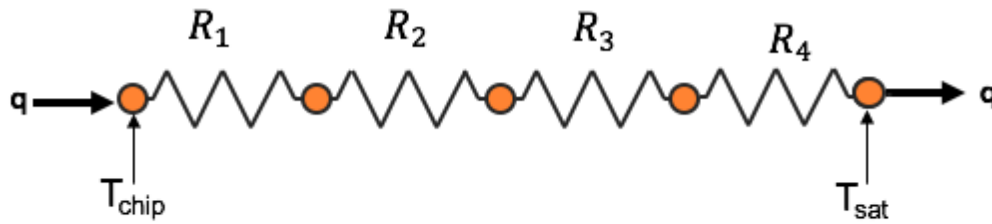
Appendix

Axial heat loss
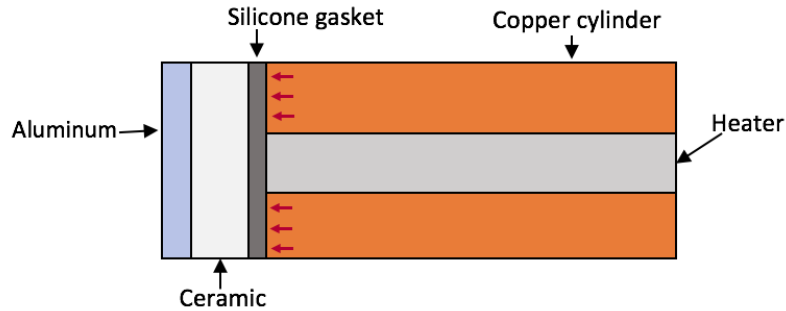
Axial heat loss would be similar in both directions. Hence heat loss is evaluated only in one direction. The cylindrical tube is covered by silicone gasket and ceramic on side for heat loss prevention followed by aluminum plate.

Resistance to axial heat transfer offered by all elements is given by,

R_1	Resistance due to silicone gasket
R_2	Resistance due to ceramic
R_3	Resistance due to aluminum
R_5	Resistance due to boiling resistance

$$R_1 = \frac{L_1}{K_1 A}$$

$$R_2 = \frac{L_2}{K_2 A}$$

$$R_3 = \frac{L_3}{K_3 A}$$

$$R_4 = \frac{1}{hA}$$

Total resistance offered, $R = R_1 + R_2 + R_3 + R_4$

Heat loss in one direction, $q = \frac{\Delta T}{R}$

Total axial heat loss, $q_{al} = 2 \times q$

Total heat loss in axial direction at minimum heat flux = 0.06%

Total heat loss in axial direction at maximum heat flux = 0.25%

Uncertainty analysis: Equations and derivations

Equations used for derivation

$q_h = V \times I$
$q_r = q_h - q_{a,l}$
$A_s = 2\pi r_2 L$
$q_r'' = \dfrac{q_r}{A_s}$
$T_{avg} = \dfrac{T_1 + T_2 + T_3 + T_4}{4}$
$T_S = T_{ave} - \left(q_r \times \dfrac{ln\dfrac{r_2}{r_1}}{2\pi kL} \right)$
$h = \dfrac{q_r''}{(T_s - T_5)}$

$$U_p = \sqrt{\sum_{i=1}^{n} \left(\frac{\partial p}{\partial a_i} u_{a_i}\right)^2}$$

Uncertainty in surface temperature

$$T_S = T_{ave} - \left(q_r \times \frac{\ln\frac{r_2}{r_1}}{2\pi kL}\right)$$

$$\frac{\delta T_s}{\delta T_{avg}} = 1$$

$$\frac{\delta T_s}{\delta q_r} = -\left[\frac{\ln\frac{r_2}{r_1}}{2\pi kL}\right]$$

$$\frac{\delta T_s}{\delta r_2} = -\left[\frac{q_r}{2\pi kLr_2}\right]$$

$$\frac{\delta T_s}{\delta r_1} = \left[\frac{q_r}{2\pi kLr_1}\right]$$

$$\frac{\delta T_s}{\delta K} = \left[\frac{q_r \ln\frac{r_2}{r_1}}{2\pi k^2 L}\right]$$

$$\frac{\delta T_s}{\delta L} = \left[\frac{q_r \ln\frac{r_2}{r_1}}{2\pi L^2 K}\right]$$

$$U_{T_s} =$$

$$\sqrt{(U_{T_{avg}})^2 + \left[\frac{\ln\frac{r_2}{r_1}}{2\pi LK}\right]^2 (U_{q_r})^2 + \left[\frac{q_r}{2\pi LKr_2}\right]^2 (U_{r_2})^2 + \left[\frac{q_r}{2\pi LKr_1}\right]^2 (U_{r_1})^2 + \left[\frac{q_r \ln\frac{r_2}{r_1}}{2\pi LK^2}\right]^2 (U_K)^2 + \left[\frac{q_r \ln\frac{r_2}{r_1}}{2\pi KL^2}\right]^2 (U_L)^2}$$

Uncertainty in radial heat flux

$$q_r'' = \frac{q_r}{2\pi r_2 L}$$

$$\frac{\delta q_r''}{\delta q_r} = \frac{1}{2\pi r_2 L}$$

$$\frac{\delta q_r''}{\delta r_2} = \frac{q_r}{2\pi r_2{}^2 L}$$

$$\frac{\delta q_r''}{\delta L} = \frac{q_r}{2\pi r_2 L^2}$$

$$U_{q_r''} = \sqrt{\left(\frac{1}{2\pi L r_2}\right)^2 (U_{q_r})^2 + \left[\frac{q_r}{2\pi L r_2{}^2}\right]^2 (U_{r_2})^2 + \left[\frac{q_r}{2\pi L^2 r_2}\right]^2 (U_L)^2}$$

Uncertainty in heat transfer coefficient

$$h = \frac{q_r''}{(T_s - T_5)}$$

$$\frac{\delta h}{q_r''} = \frac{1}{(T_s - T_5)}$$

$$\frac{\delta h}{q_r''} = \frac{1}{(T_s - T_5)}$$

$$\frac{\delta h}{T_s} = -\frac{q_r''}{(T_s - T_5)^2}$$

$$\frac{\delta h}{T_5} = \frac{q_r''}{(T_s - T_5)^2}$$

$$U_h = \sqrt{\left[\frac{1}{T_s - T_5}\right]^2 (U_{q_r''})^2 + \left[\frac{q_r''}{(T_s - T_5)^2}\right]^2 (U_{T_s})^2 + \left[\frac{q_r''}{(T_s - T_5)^2}\right]^2 (U_{T_5})^2}$$

71